The Astrophysical Journal, in press, v.550 March 20, 2001

Supernovae, Jets, and Collapsars

A. I. MacFadyen, S. E. Woosley, and A. Heger

Department of Astronomy and Astrophysics
University of California, Santa Cruz, CA 95064

ABSTRACT

We continue our study of the possible production of supernovae and a variety of high energy transients by black hole formation in massive stars endowed with rotation - the "collapsar model". The black hole may either form promptly, because a successful outgoing shock fails to be launched by the collapsed iron core (collapsar Type I), or, in a mild explosion, by fallback (collapsar Type II). In the latter case, the inner layers of the star initially move outwards, but lack adequate momentum to eject all the matter exterior to the young neutron star. Over a period of minutes to hours $\sim$ 0.1 to 5 $M_\odot$ falls back onto the collapsed remnant turning it into a black hole and establishing an accretion disk. The accretion rate, $\sim$0.001 to 0.01 $M_\odot$ s^{-1}, is inadequate to produce a jet mediated by neutrino annihilation, but similar to what has been invoked in magnetohydrodynamical (MHD) models for gamma-ray bursts (GRBs). This fallback is modeled in detail for two 25 $M_\odot$ progenitors using two different one-dimensional hydrodynamics codes - one Lagrangian and one Eulerian. The production and consequences of jets is then explored in both sorts of collapsars. Justification is given for assuming that the jet power is a constant times the mass accretion rate, $\epsilon\dot{M}c^2$, and the consequences of $\epsilon = 0.001$ and 0.01 are explored. Adopting an initial collimation half-angle of 10 degrees, the opening of the jet as it propagates through the exploding star is strongly influenced not only by the jet's kinetic energy, but by its initial pressure and the stellar structure. Cold jets tend to stay collimated, and become even more so, sometimes having an angle of only a few degrees when they reach the surface. Jets having higher internal pressure than the stellar material through which they pass, or less initial collimation, spread out and tend to make energetic, asymmetric supernovae accompanied, in helium stars, by weak GRBs. SN 1998bw may have been such an event and other events having energies between that of ordinary gamma-ray

bursts and GRB 980425 await discovery. In supergiant stars, shock breakout also produces bright x-ray transients that might be a diagnostic of the model, but even the most powerful jets (equivalent isotropic energy 10^{54} erg) will not produce a GRB in a red supergiant. For such Type II supernovae the limiting Lorentz factor is $\Gamma \approx 2$. Type II collapsars should be more frequent than Type I and may power the most common form of gamma-ray transient in the universe. However, the GRBs seen by BATSE are, for the most part, too brief to be Type II collapsars. Those are still attributed to prompt black hole formation. Even there though, the diverse energies and time structure reflect chiefly the viewing angle and the variable collimation of the jet inside the star, not a highly variable "central engine". Indeed, collapsar-induced transients may all have a common total energy in the range 10^{51} - 10^{52} erg.

Subject headings: gamma rays: bursts — stars: supernovae

1. Introduction

At the heart of current models for GRBs, one typically finds a black hole accreting rapidly through a disk (e.g., Thompson 1994; Katz 1997; Piran 1999; Mészáros 1999; MacFadyen & Woosley 1999, henceforth, MW99; Fryer, Woosley, & Hartmann 1999). Models differ in the way the hole comes to exist, in the expected accretion rate, and, especially, in the physical process(es) invoked to convert some fraction of the disk's energy into relativistic outflow. All agree, however, that some non-trivial fraction, ϵ_1, of the accreted mass-energy $\dot{M}c^2$, with $\dot{M}$ the accretion rate through the disk, goes into powering jets. In addition, some fraction, ϵ_2, of the rotational energy of the black hole ($\lesssim$9% $M_{BH}c^2$) may also be extracted in a usable form (Blandford & Znajek 1977; MacDonald et al. 1986; Mészáros & Rees 1997; Mészáros 1999; Lee, Wijers, & Brown 1999). If these sorts of models are to explain GRBs with equivalent isotropic energies of up to 10^{54} erg and $\sim$1% beaming factors using stellar mass black holes and accretion reservoirs, the total efficiency for jet formation, $\epsilon = \epsilon_1 + \epsilon_2$, cannot be much less than 1%. This is the limit realized in the most efficient neutrino powered models (Popham, Woosley, & Fryer 1999; Janka et al. 1999ab) and is conservative compared to what is often invoked for MHD-powered jets from merging neutron stars. A first-principles calculation of ϵ remains a formidable task, but an interesting interim step is to assume a constant value of ϵ and explore its consequences. That is the strategy adopted in this paper. We will manufacture jets according to a simple prescription and explore their interaction with the various stellar environments in which they may be born.

We base our calculations on the collapsar model. Previously (MW99), we explored this model as a possible explanation for common GRBs. The key element was collapse of the iron core of a rapidly rotating helium star first to a neutron star, then to a black hole (see also Woosley 1993). The black hole formed within a few seconds of iron core collapse, about the same time as infalling matter in the equatorial plane was slowed by rotation and piled into a disk. No outward moving shock was generated prior to disk formation. Henceforth, we shall refer to this model where the black hole forms promptly and makes a jet either by neutrino transport or MHD processes as a "Type I collapsar". Additional pioneering studies of the Type I collapsar were carried out by Aloy et al. (2000).

It is also quite possible to form a black hole over a longer period of time in a supernova that launches an outgoing shock with inadequate strength to eject all the helium and heavy elements outside the neutron star (Woosley & Weaver 1995; Fryer 1999). Fryer estimates that this sort of behavior might start around ~ 20 $M_\odot$ and persist up to 40 $M_\odot$. Depending upon the initial mass of the neutron star and the equation of state, the reimplosion of from ~ 0.1 to several $M_\odot$ of the stellar mantle will be adequate to produce a black hole. Excess

matter accretes into this hole, and, if it has sufficient angular momentum, forms a disk. We shall refer to this scenario as the "delayed black hole" version of the collapsar model or a "Type II collapsar". Type II is probably a more frequent event than Type I because it involves a more densely populated portion of the stellar mass function.

As we shall see (Section 2), the typical accretion rate when most of the matter falls back in a Type II collapsar is one to two orders of magnitude less than in Type I, i.e., $\sim$0.001 to 0.01 $M_\odot$ s^{-1}. This is too low for neutrinos to effectively extract disk energy and form a jet (Popham, Woosley, & Fryer 1999; MW99). However, it is similar to the accretion rate often invoked for MHD models of GRBs, especially in the case of low disk viscosity (e.g., Mészáros 1999), when $\sim$0.1 $M_\odot$ accretes in 10 s. This motivates us to consider the possibility that energetic jets will form in a supernova that is already in the process of exploding. The accretion time scale is longer than in the earlier collapsar model, but the total accreted mass and its angular momentum are comparable. If the star is a red supergiant, the jet will overtake the supernova shock before it reaches the surface, but since the velocity of the jet head is sub-relativistic, it may lose its energy input at its base before breaking free of the star. In that case, little relativistic matter would be ejected. For a helium star, however, the jet breaks out while continuing to receive accretion power at its base. Its motion may become highly relativistic (see Table 3).

The energy of the jet and the explosion it produces depend upon the efficiency of MHD processes in extracting accretion energy from the disk. As noted above, this is uncertain, but might be as large as $\sim$10%. In this paper, we shall make the simple *ansatz* that the jet power, at any point in time, is an efficiency factor, ϵ, times $\dot{M}c^2$, with $\epsilon \sim 0.001 - 0.01$ (see Section 3). Then the energy potentially available for making a jet when only one solar mass accretes is $\sim 10^{51} - 10^{52}$ erg. This conservative estimate is still large compared to the energy of a typical supernova and, if collimated into a small fraction of the sky, is also enough energy to make a powerful GRB.

Section 2 describes the initial stellar models and the one-dimensional fall-back calculations performed using the KEPLER and PROMETHEUS hydrodynamics codes. We base our calculations here on two 25 $M_\odot$ presupernova models calculated by Heger, Woosley, & Langer (2000). At sufficiently late times, the calculated accretion rate from fallback agrees well with earlier analytic estimates by Chevalier (1989). Section 3 further motivates our parameterization of the jet kinetic energy flux as $\epsilon \dot{M} c^2$ and describes some of the factors that enter into estimating ϵ.

Section 4 presents two-dimensional simulations of jet propagation in both Type I and Type II collapsars. Section 4.1 describes how the jet is initiated and introduces three additional variables (besides jet energy), namely the jet's starting radius, opening angle, and

pressure (or equivalently entropy, or the initial ratio of internal energy to kinetic energy). A fiducial opening angle of ten degrees is employed at 50 km. Since special relativity is neglected in our calculations, the initial jet is given a constant speed of 10^{10} cm s^{-1} and the density corresponding to the assumed kinetic energy flux. The jets are initiated in two different stellar configurations corresponding to collapse with high and low disk viscosity. These calculations show the degree of collimation one might expect at radii much larger than 50 km. Since it is our purpose to explore events that happen on time scales longer than can be followed with such a small inner radius (owing to the Courant condition), the results of this section provide guidance for what to use for the jets initiated at a larger radius (10^9 cm) in Section 4.2. They also show how the jet properties might vary for disks of variable viscosity and mass. The calculations here are relevant to both Type I and Type II collapsars.

Section 4.2 presents two-dimensional simulations of the response of the stellar mantle and envelope to jets assumed to have already propagated to 10^9 cm. The calculations here are carried out using as background a supernova that already launched a weak shock (Type II collapsar), but are qualitatively correct for both types since the jet is so much more powerful and travel so much faster than the supernova shock. A variety of internal energies and two different efficiency factors ($\epsilon = 0.001$, and 0.01) are explored. Jets are followed until well after they have broken free of the helium core and thus allow meaningful statements to be made regarding the final collimation and equivalent isotropic energy (given the limitations of a Newtonian study). Section 5 follows the further propagation of these jets through the hydrogen envelope of a red supergiant to breakout from stellar surface. A new inner boundary is used at 10^{12} cm. Finally in Section 6 we summarize a variety of high energy transients that might be produced by collapsars operating in different environments (see also Table 3).

2. Initial Models and Fallback

As has been known for some time (Colgate 1971, Woosley 1988), it is quite possible to produce a fairly massive black hole in an otherwise successful supernova explosion - one that would be about as bright, optically, as one that left a neutron star. Initially, the collapse of the iron core produces a neutron star and launches a shock, but, especially for more massive helium cores, the shock lacks adequate energy to eject all the matter outside the neutron star. The gravitational binding energy of the helium core increases with mass roughly quadratically while the explosion energy does not (Fryer 1999). Some portion of the matter outside the neutron star initially moves out, then falls back.

The rate of this fallback can be increased when the shock wave plows into regions with increasing ρr^3 (Bethe 1990; Woosley & Weaver 1995). So long as the shock remains in sonic communication with the origin, its deceleration in these regions is communicated back to the inner mantle, a portion of which fails to achieve escape velocity. A quantitative description of fallback must also include the *internal* energy of the ejected zones. At early times, especially a few seconds, the pressure support provided, e.g., by a piston, plays an important role. Internal energy is converted into expansion energy and zones, pushing on the piston, escape that, based solely upon their kinetic energy budget and gravitational potential, would not have. Eventually, however, the expansion becomes supersonic as the sound speed in the ejecta declines. Matter loses sonic communication with the piston and evolves independently. Careful treatments of both shock propagation and the inner boundary condition are thus essential in any study of fallback.

Heger, Woosley, & Langer (2000) have recently calculated the evolution and simulated the explosion of a grid of 15 and 25 $M_\odot$ main sequence stars, including the effects of rotation and mass loss, for several assumptions regarding efficiencies of semi-convection and rotationally induced mixing. We examine here two of their 25 $M_\odot$ models. One, with relatively inefficient semi-convective mixing, ended its life with a low density hydrogen envelope of 6.57 $M_\odot$ (Model A). The other, with more efficient mixing, had an envelope of only 1.69 $M_\odot$ (Model B). The helium core mass in each was 8.06 $M_\odot$ (A) and 8.87 $M_\odot$ (B); the iron core mass, 1.90 $M_\odot$ (A) and 1.81 $M_\odot$ (B); and the stellar radius, 8.15×10^{13} cm (A) and 8.65×10^{13} cm (B). The presupernova structure, composition, and angular momentum distribution of Model A, which will be used for most of this paper, are shown in Fig. 1. Note that Heger, Woosley, & Langer (2000) assumed rigid rotation on spherical shells, hence the actual angular momentum in the equatorial plane is 50% higher than the angle-averaged value in Fig. 1). Both models had sufficient angular momentum to form a Kerr black hole in the center and for the matter in the equatorial plane to form an accretion disk around it. That is, there is sufficient angular momentum available for the black hole to stay at maximum rotation, and the angular momentum in the equatorial plane is high enough to stop infall at the last stable orbit (in co-rotation) around a Kerr black hole.

For this paper, we calculated a new series of supernova explosions based upon the models of Heger et al., but with a range of kinetic energies at infinity (Table 1). The explosion was simulated by a piston that first moved inwards for 0.45 s until it reached a radius of 500 km and then moved outwards with an initially highly supersonic velocity. This velocity was decelerated like a test particle in the gravitational field of central mass of $\alpha_{\rm pist}$ times that of the core. For Model A the assumed core below the piston was 1.97 $M_\odot$ and for Model B, 1.84 $M_\odot$. The initial velocity was chosen so that the piston came to a rest at 10,000 km (Woosley & Weaver 1995; Heger, Woosley, & Langer 2000). An exception

was Model A17 in which a terminal radius of 100,000 km was assumed for comparison.

None of these were "failed supernovae" in the sense described by Woosley (1993) and MW99. While neutrino transport was not modeled, the motion of the piston gave an outgoing shock that, even for the the lowest energy considered, ejected at least the hydrogen envelope of the star with supernova-like speeds. Each of the models in Table 1 would have had made a bright Type II supernova without any additional energy input, though many would have lacked the characteristic "radioactive tail" from ^{56}Co decay. For piston trajectories that give kinetic energies at infinity above about 1.2×10^{51} erg, calculations by Blinnikov (1999) have shown that the high mass envelope star (Model A) would produce a rather typical Type IIp supernova. The low mass envelope gives a curve more like a Type II-L supernova (Model B).

However, especially for energies below $\sim 1.0 \times 10^{51}$ erg, large amounts of material failed to escape and fell back to the center of the explosion. Fallback masses ranged from approximately zero to essentially the entire helium core (Table 1). The accretion was followed in some detail using two quite different codes: one, the same one-dimensional Lagrangian hydrodynamics code, KEPLER (Weaver, Zimmerman, & Woosley 1978), used to simulate the presupernova evolution and the explosion. The other was a one-dimensional version of the Eulerian code, PROMETHEUS (Fryxell, Müller, & Arnett 1989, 1991; MW99). PROMETHEUS is an implementation of the high order Godunov hydrodynamics scheme, PPM (**p**iece-wise **p**arabolic **m**ethod), and we shall henceforth refer to PROMETHEUS as "the PPM code".

The effect of various inner boundary conditions on the fallback was then studied. In KEPLER, the inner boundary was the piston zone, held fixed at its final radius, usually 10,000 km. Material that fell back, accumulated and came to rest. It was distinguished from outgoing material by having velocity less than 100 km s^{-1} and a large positive velocity in the next zone out.

When the same calculations were repeated using PPM, the results depended sensitively upon the treatment of the inner boundary condition and the time the calculation was linked from KEPLER. For a transmitting boundary condition (zero radial gradient of all variables), initiated as the shock left the carbon-oxygen core (10 s after core bounce), a rarefaction overtook the outgoing matter and more matter fell back than in the equivalent KEPLER calculation. For example, fallback in Model A11 was increased from 0.47 $M_\odot$ in the KEPLER calculation to 1.0 $M_\odot$ in the PPM calculation, and the explosion energy at 10,000 seconds was reduced from 1.21 $\times 10^{51}$ ergs to 1.08 $\times 10^{51}$ ergs.

It is not physical for the matter to rest on the piston, nor is it physical to remove all

pressure support from the model while the explosion is still developing. We thus sought a compromise. Fig. 3 shows the radial location of Lagrangian zones as a function of time for the KEPLER (piston-driven) explosion of Model A01. Fig. 2 provides an important detail, regions in the presupernova star where an outgoing shock wave is expected to speed up or slow down. While initially ($t \lesssim 60$ s) all zones are moving rapidly outwards, by about 100 s a bifurcation appears and, by 250 s, 2.6 $M_\odot$has fallen back onto the piston. This material would collapse to the origin were the piston removed. We thus chose to make our link for Model A01 to PPM at 100 s, using a transmitting boundary condition thereafter. This resulted in good agreement between the total fallback rate calculated with the two codes (Table 1), while the PPM calculation more physically described the fallback of matter to the origin at late times.

In addition to the need for hydrodynamical matching between the two codes, the mapping at 100 s also has a physical basis. During approximately the first 10 s, a neutrino driven wind powered by the radiating proto-neutron star pushes against the outgoing stellar mantle and prevents its reimplosion. Eventually, however, post-shock gas which has failed to achieve escape velocity is pushed back toward the proto-neutron star, both by gravity and an inwardly-directed pressure gradient. This falling material overcomes the resistance of the low density neutrino heated bubble and penetrates, perhaps by forming "fingers", back to the hard surface of the neutron star where it accumulates in an atmosphere on top of the hard neutron star surface (Fryer, Benz, & Herant 1996, Chevalier 1989). For the accretion rates relevant for the first $\approx$ 100 s (Fig. 5), an "atmosphere" builds up out to several hundred kilometers, at which point neutrino cooling behind the shock balances the accretion energy deposition rate and accreting gas settles subsonically onto the neutron star. By 100 s after core collapse, enough gas has fallen back for weak explosion energies (especially for Models A01 - A03) that the neutron star collapses to a black hole. For intermediate explosion energies the central object may still be a neutron star, but the accretion rate is such that the accretion shock forms interior to our inner boundary at 10^9 cm so that gas near the boundary is in free fall and the neutral inner boundary condition is justified. Only for accretion rates below a few times 10^{-6} $M_\odot$ s^{-1}, not considered here, would the accretion shock move out beyond 10^9 cm and the boundary condition would have to be modified.

Once a black hole has formed, gas that falls back with sufficient angular momentum will settle into a disk. While this part of the star is not modeled in the current calculations, Popham et. al. (1999) and MW99 found that the inner disk can transport the mass it receives from the collapsing star in a steady state. An accretion shock forms near the Keplerian support radius of the accreting gas, typically several hundred kilometers. The upstream collapsing star is unaware of the accretion disk and collapses in free fall exterior

to this region. An exception is outflows which can develop for high viscosity ($\alpha \gtrsim 0.1$) disks (MW99). These outflows are not treated in the present simulations. Since we consider accretion rates lower by one to three orders of magnitude than in MW99 and since the MHD processes assumed to power the jets can operate with low disk viscosities (unlike neutrino annihilation models), the absorbing boundary condition at 10,000 km is acceptable for these calculations. Future work will address disk outflows in detail for the case of high viscosity disks, including calculation of the nucleosynthesis.

The accretion rates obtained from the PPM calculations are plotted as a function of time in Fig. 5. The characteristic time for half the mass to fallback is given in Table 1. Accretion rates between 10^{-4} and 10^{-2} $M_\odot$ s^{-1} are maintained for hundreds to thousands of seconds.

Accretion onto collapsed objects inside of supernovae has been considered previously in a semi-analytic fashion by Chevalier (1989) who pointed out, for the high accretion rates considered here, that accretion onto a neutron star would be mediated by neutrino losses (see also Fryer, Benz, & Herant 1996 and Zampieri et al. 1998). Unless the neutron star magnetic field is unusually strong, the accretion rates we are interested in are sufficiently high that the neutron star magnetic field would be crushed to the surface and sufficiently low so as not to launch a second supernova shock by neutrino absorption. Chevalier gives an approximate formula for the fallback accretion rate based on the parameters of SN 1987A and assuming a time sufficiently late that the "reverse shock" has already reached the center:

$$\dot{M} = 1.0 \times 10^{35}\, t^{-5/3} \text{ g s}^{-1} .$$

For models with large amounts of fallback, our calculations show that accretion occurs without the mediation of a strong "reverse shock". Indeed, it is not possible for the reverse shock in a red supergiant to make it back to the center of the star in only a few hundred seconds. Consequently, Chevalier's formula becomes applicable much earlier than the 10^4 s he estimated for SN 1987A. However, different regions of the star have variable entropy, in particular jumps at the boundaries of active burning shells and convective shells. One large jump is located at the oxygen burning shell in the presupernova star. As a result, one sees in Fig. 5, an early high accretion rate that slows abruptly after the silicon shell has fallen in (mass coordinate $2.6\,M_\odot$ in the presupernova star). After that point though, during the accretion of the carbon-oxygen core, $\sim$ 400 s in Model A04, the accretion rate does start to decline roughly as $t^{-5/3}$ and is in rough quantitative agreement with Chevalier's estimate for SN 1987A.

3. Jet Energy

From many observations of all sorts of situations where material accretes from a disk into a compact object – star forming regions, active galactic nuclei, microquasars, SS-433, and planetary nebulae – it seems that jets are a ubiquitous phenomenon (e.g., Livio 1999; Pringle 1993). In each of these phenomena, the jet typically carries away from ∼3% to 30% of the binding energy of the disk and the jet speed is of order the escape velocity. For jets produced near the event horizon of an accreting black hole, the relevant speed is the speed of light. In the case of black hole accretion, one also has the advantage of knowing the binding energy of the last stable orbit as a function of Kerr parameter and black hole mass. The rate at which matter flows through that last stable orbit and liberates some of this energy in a useful form is just given by the accretion rate. This suggests writing the power of the jet in a simple parametric form $\dot{E}_{\rm jet} \; = \; \epsilon \dot{\rm M} c^2$.

For example, for the Blandford-Znajek (1977) process for extracting rotational energy from a black hole with Kerr parameter $a \equiv Jc/GM^2$ predicts:

$$\dot{E}_{\rm jet} \; \approx \; 3 \times 10^{51} \, a^2 \left(\frac{\dot{\rm M}}{0.1 \; {\rm M}_\odot \; {\rm s}^{-1}} \right) \; {\rm erg \; s}^{-1},$$

or in terms of our efficiency parameter, $\epsilon \approx 0.01 \, a^2$. This assumes the development of a nearly equipartition magnetic field, about 10^{15} gauss for stellar mass black holes.

A similar expression that makes the dependence upon magnetic field strength explicit is given by McDonald et al. (1986),

$$\dot{E}_{\rm jet} \; \approx \; 10^{50} \, a^2 \left(\frac{\rm M_{BH}}{3 \, {\rm M}_\odot} \right)^2 \left(\frac{\rm B}{10^{15} {\rm gauss}} \right)^2 \; {\rm erg \; s}^{-1}.$$

To illustrate the uncertainties involved, we consider a steady state disk with accretion rate $\dot{\rm M} = 4\pi {\rm rH}\rho {\rm v}$, with H, the disk scale height and v, the radial velocity. The viscous time scale is approximately $\tau = r^2/\alpha H^2 \Omega_K$, with α, the disk viscosity parameter and Ω_K, the Keplerian angular velocity. Further, assuming a fraction, δ, of the equipartition magnetic field energy density, $B^2/4\pi \sim \delta \rho \Omega_k^2 r^2$, an advection dominated disk with $H \sim \beta r$, and a disk radius where the energy is mostly generated equal to γ times the Schwarzschild radius, a similar relation is again found between the jet energy and accretion rate,

$$\dot{E}_{\rm jet} \; \sim \; 0.02 \left(\frac{a}{0.5} \right)^2 \left(\frac{0.5}{\beta} \right)^3 \left(\frac{3}{\gamma} \right)^{2.5} \left(\frac{\delta}{0.01} \right) \left(\frac{0.01}{\alpha} \right) \; \dot{\rm M} c^2.$$

This formula makes clear the sensitive dependence of ϵ on a number of uncertain parameters while indicating that $\epsilon \sim 0.001$ to 0.01 is a reasonable choice.

Similar powers can also be produced by the magnetosphere of the accretion disk and by winds accelerated by viscous dissipation in the disk (MW 1999; Stone, Pringle, & Begelman 1999). In fact, these powers may dominate the energy extracted from black hole rotation in most situations of interest (Blandford & Znajek 1977; Livio, Ogilvie, & Pringle 1999). There, one also expects the energy extraction to scale with the energy density in the magnetic field (times the disk area and Alfven speed). Using the same assumptions as the previous paragraph, this situation also gives a jet luminosity that scales as $\dot{M}c^2$.

4. Two-Dimensional Simulations of Jet Propagation

Given a prescription for the jet power and a background star in which to propagate it, one can then model the interaction of the jet with the star.

As a matter of convenience, we separate our discussions and calculations into two regions, one inside 10^9 cm, another from 10^9 cm to the surface of Model A01 at 8.15×10^{13} cm. This segregation reflects, in part, the difficulty of carrying too large a dynamic range on the computational grid. Time steps imposed by the Courant condition at, e.g., $\sim 10^7$ cm, are too small to follow the progression of the explosion to the surface at $\sim 10^{14}$ cm. The split also separates the problem into regions of different physics. In the inner region, the jet forms, with all the attendant uncertain physics that involves. The outer region, however, contains the bulk of the mass and volume of the star. Occurrences inside 10^7 cm are discussed in Section 4.1. The numerical models presented there are still subject to the Courant restriction which makes it difficult to follow fallback for hundreds, or even thousands of seconds, so our arguments in Section 4.1 are based upon the stellar and disk structure calculated for Type I collapsars in MW99. Expected differences between Type I and Type II are discussed, but we are mainly interested in this region as providing reasonable inner boundary conditions for the outer region treated in Section 4.2.

In the outer region, the jet may be defined by an (angle-dependent) flux at the inner boundary of energy and density. Studies of this region will show how jets of different properties affect the star through which they propagate, in particular how much energy is shared with the star, whether the jet suffers degradation or additional collimation, and the degree to which relativistic matter is ejected. Note that though the results of Section 4.2 are discussed within the context of the collapsar model for GRBs, they are equally appropriate to any model that produces jets with similar properties, for example jets powered by a highly magnetic, rapidly spinning neutron star (Usov 1994; Wheeler et al. 1999, Khokhlov et al. 1998).

4.1. Jet Initiation

A variety of processes may operate in the vicinity of a rotating black hole to create a jet. Very close to the hole, magnetic fields maintained by currents in the disk and threading the black hole ergosphere can extract rotational energy — the Blandford-Znajek (1977) mechanism. Farther out, other MHD processes may also extract angular momentum and energy from the disk to form a jet, e.g., by magneto-centrifugal forces (Blandford & Payne 1982). See Koide, Shibata, & Kudoh (1998), Meier (1999), Koide et al. (1999) and Krasnopolsky, Li, & Blandford (1999) for recent discussions. These processes tend to produce relatively cold jets, in the sense that the thermal energy of the jet is not initially large compared to either the rest mass or the jet kinetic energy. There may be a critical magnetic field above which these mechanisms are able to provide directly matter with high Lorentz factor (Meier et al. 1997). Other processes like neutrino energy deposition (Woosley 1993; MW99; Janka et al. 1999ab) or magnetic reconnection (Thompson 1994; Katz 1997) in the disk deposit their energy chiefly as heat and make hot jets. In these cases the initial velocity of the jet is small and asymptotic velocity is given by the initial ratio of thermal energy to rest mass. Because the pressure from the deposited energy is initially isotropic, the collimation of hot jets then occurs as a consequence of the pressure and density gradients of the matter in which energy is deposited. Cold MHD jets may thus be collimated both by magnetic fields and by geometry, but hot jets are collimated only by the structure of the medium in which they expand.

The jets of MW99 are hot jets, focused by the thick accretion disk and declining radial pressure gradient in the region where energy was deposited. In order not to obtain a velocity greatly in excess of the speed of light in their Newtonian code, MW99 were restricted to depositing energy at a rate that, in steady state, gave an internal energy to baryon loading less than 10 times the rest mass (even this gave speeds of over 10^{11} cm s^{-1}!). These jets easily penetrated the helium core in which they were produced while concurrently blowing it up, but details of shock break out, and especially a first principles determination of the asymptotic Lorentz factor of the jet, were obscured by use of a hydrodynamics code that was not special relativistic. More recently, Aloy et al. (2000) (see also Müller et al. 1999) have recalculated the MW99 conditions using a fully relativistic version of the PPM code (Aloy et al. 1999) and obtained similar results - i.e., relativistic jet penetration of the helium core. In addition, they were able to determine that, *at breakout*, Lorentz factors of 20-30 were achieved in the jet. It is expected that higher values may be achieved by running the calculation longer. These hot jets were all in the context of a Type I collapsar.

It is not clear whether the jets made by fallback in a Type II collapsar will be hot or cold (although jets mediated by neutrino transport are impossible). Given the continuing

limitations of our Newtonian treatment, we can only explore the physics of mildly relativistic "warm" jets. However, we can vary such things as the kinetic energy and internal energy loading of the jet, its initial collimation, and the mass and structure of the accretion disk in which it propagates in order to understand better how the jet is dynamically focused.

As an example, we consider jets initiated in the two accretion disk structures studied by MW99, a high viscosity disk (Model 14A, $\alpha = 0.1$, their Fig. 8 at 7.6 s) and a low viscosity disk (Model 14B, $\alpha = 5 \times 10^{-4}$, their Fig 22 at 9.4 s). The masses of these disks differ by approximately a factor α^{-1}, a few hundred. One might expect a similar difference in disk mass for constant viscosity, but reducing the accretion rate by a few 100 (Popham et al. 1999). We use the same constant energy injection rate for both disk structures to isolate the effect of the disk structure on the jet collimation. This injection rate is therefor not directly determined by the accretion rate from the disk calculation but it corresponds to $\epsilon = 0.1$ for the accretion rates of $\sim 0.1 M_\odot$ s^{-1} characteristic of the disk calculations (see MW99). The difference between jet behavior initiated in these two models qualitatively illustrates the effect we expect for the high accretion rate in Type I collapsars and the two order of magnitude lower accretion rate in Type II collapsars.

Jets were initiated in both models at an inner boundary radius of 50 km, with an opening half-angle of 10 degrees, a velocity of 10^{10} cm s^{-1}, and a total power of 1.8×10^{51} erg s^{-1}. The jets were initiated about 10 s after core collapse, 7.6 s for Model 14A and 9.4 s for 14B at a time when the disks had fully formed. Gas was still infalling along the polar axis when the jets were initiated, but the flow was easily reversed given the energy injection rate employed (see MW99, §5 for the appropriate criterion). At later times (t $/gtrsim$100 s), as fallback continues the jet has passed the supernova shock and has cleared a path along the polar axis the ram pressure of the infalling gas decreases as $t^{-5/3}$ and provides

Half of the injected energy was in kinetic energy and the other half in internal energy. The energy to rest mass ratio was thus about 10% so as to avoid super-luminal velocities on the grid. Figs. 7 and 8 show the results after 0.6 s of jet propagation.

Both calculations clearly show the effect of geometric focusing, but the jet in the lower mass accretion disk is much less collimated. Since the sub-relativistic gas has comparable internal and kinetic energies, the sound speed is near the radial streaming speed, so one expects the jet, in a vacuum, to have comparable theta and radial velocities. This is initially the case for the calculation using the low disk-mass. After a thousand km, the opening half-angle is about 20 degrees. The pressure gradient of the star is still enough to maintain some mild collimation. In the high disk-mass case though, the opening angle is about half as great, comparable to the 10 degree input angle. If one continued this trend to still

smaller disks and higher internal energy loading factors, the jet would fan out still more. Obviously, in the limit of no disk and energy deposited entirely as a thermal bomb at the middle, an isotropic explosion would develop. An interesting question still to be explored is what would happen in the absence of a disk, but for off-center energy deposition.

The calculations of MW99 (their Fig. 26) showed that the ratio of internal energy to mass density in the jet declined roughly as $r^{-1/3}$. That is, the density declined between r^{-1} and r^{-2} and the radiation entropy, T^3/ρ, was constant. For constant mass flux, constant velocity, and constant opening angle, θ, the quantity $\pi r^2\theta^2\rho v$ should be a constant, so that $\rho \propto r^{-2}$. That the density declined more slowly reflects the hydrodynamical collimation and mild deceleration of the jet. Assuming that the $r^{-1/3}$ scaling persists for much lower values of initial internal energy, one expects the ratio of internal energy to kinetic energy to decline by about a factor of 10 going from the region where the jet forms out to 10^9 cm. So for jets that initially had from, say, 1% to 100% of their initial energy in the form of radiation, the ratio of pressure to kinetic energy, f_P, at 10^9 cm would be in the range 0.001 - 0.1. We shall use these values in the next section. For much hotter jets, the effects of special relativity (especially the contribution of pressure to momentum) make the above scaling law invalid and the jets stay much more tightly collimated than a non-relativistic calculation would suggest (Woosley, MacFadyen, & Heger 1999; Müller et al. 1999; Aloy et al. 1999, 2000). For much cooler jets we shall find that the answer does not vary much for f_P less than 0.01 (Fig. 10).

4.2. Jet Propagation and Supernova Explosion in Type II Collapsars

The spherically symmetric explosion of Model A01, followed until 100 s after the launch of a weak shock in the KEPLER code (Section 2), was mapped onto the Eulerian grid of a two-dimensional version of the PPM code. This grid used 200 radial zones spaced logarithmically between an inner boundary at 10^9 cm and the stellar surface at 8.1×10^{13} cm. Forty angular zones, concentrated near the pole, were used to simulate one quadrant of the stellar volume, assuming axial and reflection symmetry across the equatorial plane. The angular resolution varied from 1.25° at the pole to 3.5° at the equator. Nine atomic species, (C, O, Ne, Mg, Si, Fe, He, n, p), were carried and the equation of state included radiation and an ideal gas consisting of electrons and the nine ions. At 100 s, the inner 1.99 $M_\odot$ of the star was removed and replaced by a transmitting (zero radial gradient of all variables) boundary condition at 10^9 cm. The 1.99 $M_\odot$ and all subsequently accreted matter contributed to a point mass term in the gravitational potential which was calculated using an integral Poisson solver (Müller & Steinmetz, 1995, MW99). At this time, the weak

initial shock was already at 1.1×10^{10} cm when a simulated jet was turned on at the inner boundary.

A given jet powered model was specified by its energy flux, $F_{\rm e}(t)$, mass flux, $F_\rho(t)$, momentum flux, $F_{\rm u}(t)$, and the pressure of the jet, $P_{\rm jet}$, all at 10^9 cm,

$$F_{\rm e} = \dot{E}_{\rm jet}(t)/A_{\rm jet} \quad (1)$$

$$F_\rho = 2{\rm F_e}\left[f_{\rm P}\left(\frac{1}{\gamma_{\rm jet}-1}+1\right)+1\right]^{-1} v_{\rm jet}^{-2} \quad (2)$$

$$F_{\rm u} = F_\rho v_{\rm jet} \quad (3)$$

$$P_{\rm jet} = \frac{1}{2} f_{\rm P} F_{\rm u} \quad (4)$$

with

$$\dot{\rm E}_{\rm jet}({\rm t}) = \epsilon {\rm c}^2 \times \begin{cases} \dot{\rm M}(t) & : \quad t < t_{\rm p} \\ \dot{\rm M}(t_{\rm p}){\rm max}[({\rm t/t_p})^{-5/3}, 10^{-6}] & : \quad t \geq t_{\rm p} \end{cases}$$

Here $t_{\rm p}$ is the time when the accretion rate begins to follow the power law decline, usually several hundred seconds (Fig. 5). The opening half-angle of the jet was taken to be $\theta_{\rm jet} = 10^\circ$ and the adiabatic index, $\gamma_{\rm jet} = \frac{4}{3}$. The accretion rate $\dot{\rm M}$ was restricted to that matter that fell in through the inner boundary within 45° of the equator. Thus the density of the jet is given by $2\epsilon\dot{\rm M}c^2/((4f_{\rm P}+1)A_{\rm jet}v_{\rm jet}^3)$ where $A_{\rm jet}$ is the cross sectional area of the initial jet, 1.9×10^{17} cm^2 for the assumed boundary radius and collimation. The assumed initial velocity of the jet, $v_{\rm jet}$, was 10^{10} cm s^{-1}.

We considered four cases, $\epsilon = 0.001$, $f_{\rm P} = 0.001$, 0.01, and 0.1, and $\epsilon = 0.01$, $f_{\rm P} = 0.01$. The results of these calculations are summarized in Table 2 and Figs. 9 - 11. Here the model naming follows the convention "JMN" where "J" indicates the model included a jet, but was otherwise based upon the initial Model A01 (Table 1), "M" is the exponent of the efficiency factor, $\epsilon = 10^{-{\rm M}}$, and "N", the exponent of the pressure factor, $f_{\rm P} = 10^{-{\rm N}}$. The accreted mass, ΔM in Table 2, is smaller than the 3.71 $M_\odot$ computed without a jet (Fig. 5 and Table 1) for Model A01, because the jet impeded the accretion at high latitude and because the accretion was not quite complete after 500 seconds (Fig. 5). The total energy input by the jet was still $\epsilon\Delta{\rm M}c^2$, but the energy in Table 2 was also reduced by the work done up to 500 s in unbinding the star and by the internal and kinetic energy which passed inside the inner boundary. The 2.55×10^{50} erg due to the initial shock has been subtracted in Table 2 so that $E_{\rm tot}$ reflects only the energy input by the jet.

In all cases a very energetic asymmetric supernova resulted. Since the integrated mass of the jet in our code was comparable to that of the stellar material within 10 degrees, the

time for jet break out was approximately the stellar radius divided by the jet input speed, or about 8000 s. Since the energy of the jet engine had declined greatly by that time, due to the declining accretion rate (Fig. 5), the jet that broke out was only mildly relativistic (see also Section 5). Both the long time scale and the small amount of relativistic matter are inconsistent with what is seen in common GRBs. However, if the hydrogen envelope had been lost leaving a bare helium star, a longer than typical GRB could have resulted.

Figs. 10 and 11 illustrate how the pressure balance between the jet and the star through which it propagates affected its collimation properties. The interaction at late times with the hydrogen envelope has a smaller effect on the angular energy distribution which was set chiefly by $f_{\rm P}$ and the interaction with the helium core. Model J33 had the lowest internal pressure (note that the actual value of the initial pressure depends upon the product of ϵ and $f_{\rm P}$). The final jet was collimated even more tightly than given by its initial injection. That is, a jet initially of 10 degrees half width will exit the star with a FWHM of less than two degrees, about 0.06% of the sky, though the angular resolution of the code is questionable for such small angles. Meanwhile the energy at larger angles was not much greater than that given by the initial, weak spherically symmetric explosion, $10^{50.4}$ erg. There was little sharing of the jet energy with the star and, except for the jet, the supernova energy remained low.

This behavior is to be contrasted with Models J22 and J31 where the jet collimation was weaker and much more energy was shared with the star. Note that though Model J22 had about 6 times the total energy of J31 owing to its larger ϵ, the fraction of energy at large angles in both these models was significantly greater than in Models J32 and J33. That Model J22 was not ten times more energetic (the ratio of the ϵ's) shows the inhibition of the accretion by the strong jet. Still, Model J22 would be a very powerful supernova as well as one accompanied by a jet.

As the jet pushes through the star, a shell of relatively high density material is built up at its head. The shell contains material from the inner regions of the star which is swept along as the jet propagates through the star. The red regions near the polar axis in Fig. 10 correspond to the location of the shells. If some of this material is accelerated to relativistic velocities by the jet, as preliminary relativistic calculations indicate (Aloy et al. 2000), it may produce observable features in the spectrum of the burst. More work is needed, however, to determine the detailed composition of the jet material at large distances from the center of the star.

The angular factor R($\theta > 10^\circ$) in Table 2 is the ratio of the integral of the kinetic energy due to the jet outside 10 degrees polar angle (98.5% of the sky) to the total kinetic energy in the star due to the jet (see Fig. 11). These energies were computed by taking

the total kinetic energy at 400 s after jet initiation in both regions and subtracting the kinetic energy of the initial supernova shock. R($\theta > 10°$) measures the extent to which the jet spread laterally and shared its energy with the rest of the star. The limiting case, R($\theta > 10°$) = 0, would correspond to a jet that shared none of its energy with the supernova outside an initial 10° polar angle. This sort of behavior is expected for "cold" jets with internal pressure small compared to the exploding helium core. The other extreme, where the jet shared its energy evenly with the entire star and produced a spherical explosion, would correspond to R = $\cos\theta$ = 0.985. Our "hot" jets lie somewhere between these two limits. The quantity R($\theta > 20°$) was similarly computed for a polar angle of 20°. The isotropic limit there would be 0.940.

Most of the curves in Fig. 11 were evaluated at a time (500 s) when the central part of the jet had moved well outside the helium core (initial radius 5.0×10^{10} cm - defined by the point where the mass fraction of hydrogen is 1%), but had not yet encountered much of the hydrogen envelope mass. Thus the energy distribution is also appropriate to exploding helium stars of mass ∼9 $M_\odot$. These curves then give the angular energy distribution of Type Ib and Ic supernovae that would accompany GRBs produced by jets of the specified properties.

For one calculation, J32, however, the propagation beyond 500 s was considered all the way to the surface of the red supergiant at 7820 s ($\sim R/v_{\rm jet}$; note the near constancy of the jet head speed in the hydrogen envelope). This calculation required a second mapping of the explosion onto a new grid. At 500 s a new inner boundary was set up at 10^{11} cm to alleviate the restrictive time step limitation imposed by the Courant condition at small radii. The mass interior to the new inner boundary was added to the central point mass. 150 radial zones spaced logarithmically between 10^{11} cm and $8{\times}10^{13}$ cm were used with the same angular zoning as before. At 500 s the bulk of the accretion had already taken place (Fig. 6) and the subsequent accretion could be approximated using the $t^{-5/3}$ scaling at late times (Fig. 5), $\dot{M}(t) = \dot{M}(500\,s) \times \max[(t/500)^{-5/3}, 10^{-4}]$. The jet was injected as a boundary condition at the new inner boundary, $r = 10^{11}$ cm, as before with $\theta_{jet} = 10°$ and with $v_{jet} = 1 \times 10^{10}$ cm s^{-1}. $f_{\rm p}$ was reduced to 10^{-3} to approximate the conversion of thermal energy to kinetic energy which occurs as the gas expands adiabatically between 10^9 cm, where $f_{\rm p}$ was previously 0.01, and 10^{11} cm.

The results of this calculation at the time of jet breakout are shown in Fig. 12. Note the lateral propagation of a strong, high Mach number shock with a large pressure and density jump. This shock wraps around the star and, by about 10,000 s, has ejected even the material in the equatorial plane. The jet core spreads significantly out to about 10^{13} cm, well into the hydrogen envelope, but then is recollimated by a "cocoon" of high pressure,

shock heated gas. Further out at 5×10^{13} cm, it spreads once again due to partial blockage by a plug of high density material which the jet shoves along.

Though these calculations of jet propagation were carried out against the background of supernova already experiencing a weak explosion, the area per unit solid angle of the jet is so large and its speed so great that it rapidly overtakes and overwhelms the initial shock. Thus, qualitatively, the results of this section, including Table 2 and Figs. 9 - 11, would also apply to Type I collapsars.

5. Shock wave Break Out

A strong shock wave breaking out of a star that is experiencing mass loss will produce transient electromagnetic emission in two ways - first as the shock breaks through the surface and exposes hot material (Colgate 1969, 1974), and second as the highest velocity material encounters the circumstellar wind (Chevalier 1982, Fransson 1984, Leising et al. 1994). While the highest energy ejecta in the present models may only have a small solid angle (Fig. 11), there still may be a very high luminosity in both forms of transients. This radiation would not be appreciably beamed.

To explore this possibility, we compute the effects of two strong, spherically symmetric shocks in Model A01 using the KEPLER code. The motion of the piston at the edge of the iron core (see Section 2) was adjusted to give both models very high kinetic energy at infinity, 1.44×10^{53} erg and 1.39×10^{54} erg. While these were one-dimensional calculations, they should simulate the conditions experienced by stellar regions within solid angles that experience these "equivalent isotropic energies" (Fig. 11). The advantage of the one-dimensional Lagrangian calculations is that very fine zoning can be employed near the surface and radiative diffusion can be included in the calculation.

The resulting light curves for the two models are given in Fig. 12. Since KEPLER has a very simple radiation transport scheme (flux-limited radiative diffusion) and the opacity is dominantly due to electron scattering, the effective temperature obtained in these calculations is an underestimate of the actual (color) temperature, T_c, by a factor of two to three (Ensman & Burrows 1992). Thus we expect, for the higher energy model, a transient with mean photon energy, $3\ kT_c \sim 0.25$ keV lasting for about 10 s. Since these x-rays would not be beamed, the luminosity would be the value in Fig. 12 times an appropriate solid angle (about 1% of the sky), or $\sim 10^{47}$ erg s^{-1}. Less energetic, but longer lasting transients would come from regions of the surface that experienced a smaller equivalent isotropic energy. This is much brighter and harder than the shock breakout transients expected from

common Type II supernovae and would be a diagnostic of our model.

Even more energy may come out, but over a longer time, in the form of x-ray and radio afterglows from circumstellar interaction. KEPLER is a non-relativistic hydrodynamics code, but we can nevertheless estimate the amount of relativistic ejecta following Woosley, Eastman, & Schmidt (1999). Assuming the near constancy of the quantity $\Gamma\beta(\rho r^3)^{1/5}$ (with $\beta = \mathrm{v/c}$ and $\Gamma = (1-\beta^2)^{-1/2}$) across the mildly and strongly relativistic domains (Gnatyk 1985; McKee & Colgate 1973), we obtain Γ as a function of the external mass using the output of KEPLER in the non-relativistic region (Fig. 14). The finest zones in the KEPLER calculation had mass 10^{29} g. However, external to about 10^{31} g the density was influenced by a transition from optically thick to optically thin zones, and outside of 10^{30} g, the density was affected by a 3 dyne cm^{-2} surface boundary pressure employed to stabilize the calculation. We thus only trust the calculated distribution of ρr^3 out to 10^{31} g and expect that there may be relatively minor deviations from that power law outside. Of course, we also cannot employ zones in our fit which in the KEPLER calculation were moving at super-luminal speeds after the conversion of all internal energy to kinetic energy.

For these reasons, we used only the KEPLER results inside 10^{31} g and used a power law extrapolation for smaller masses. The fits for $\Gamma\beta(\rho r^3)^{1/5}$ gave nearly constant value of 7.3×10^5 and 3.3×10^6 (units g$^{1/5}$) for the 1.44×10^{53} and 1.39×10^{54} erg explosions respectively. From these we infer the distribution of Γ with exterior mass given in Fig. 14 for the high energy explosion. Much less relativistic matter was ejected in the lower energy explosion.

One cannot use the scaling relation for Γ indefinitely though. Especially for extended objects like red supergiants, there comes a point when the shock thickness, mediated by radiation and electron scattering, becomes greater than the density scale height. At about the same point, material behind the shock will become optically thin and lose energy. For relativistic shocks, both of these conditions occur when the Thompson depth of material just behind the shock becomes unity (Imshennik & Nadyozhin 1989). From the known dependence of ρr^3 on external mass (Fig. 14), $\rho r^3 = 10^{5.31}(\Delta \mathrm{M\,(g)})^{\delta}$ with $\delta = 0.86$, one determines the external mass beyond which the shock speed cannot be extrapolated

$$\Delta \mathrm{M} \;=\; 2.0 \times 10^{29} \left(\frac{R_*}{10^{14}\ \mathrm{cm}}\right)^2 \left(\frac{\delta}{0.86}\right) \left(\frac{0.34\ \mathrm{cm^2\ g^{-1}}}{\kappa}\right)\ \mathrm{g},$$

where R_* is the stellar radius. For the much more compact stars considered by Woosley, Eastman, & Schmidt (1999), small amounts of material can be accelerated to comparatively large values of Γ, but here, for red supergiants, there is a limit of $\Gamma \approx 2.5$. Thus jet powered Type II supernovae cannot make GRBs of the common type. The duration of the jet is too short for the jet itself to acquire large Γ outside the star and the relativistic shock

acceleration mechanism fails to yield sufficiently energetic material.

However, 10^{-4} $M_\odot$ of material with $\Gamma = 2.5$ is still about 10^{50} erg of kinetic energy. This material will radiate its kinetic energy after encountering roughly its rest mass, which will take a time

$$\tau \; = \; 10^4 \; \left(\frac{10^{-5} \; M_\odot \; y^{-1}}{\dot{M}} \right) \left(\frac{10 \; km \; s^{-1}}{v_{wind}} \right) \; s.$$

For a solid angle 1% of the sky, this again implies $\sim 10^{44}$ erg s^{-1}, presumably in hard x-rays. In fact, the circumstellar interaction of these breakout shocks resembles in many ways the multi-wavelength afterglow of GRBs, except that there would be no GRB. Since these could be frequent events and may not be beamed to the same small angle as a GRB, there could be many such "orphan afterglows".

6. Conclusions

It is widely believed that many diverse phenomena in galactic nuclei – quasars, BL-Lac galaxies, Seyferts, radio galaxies, blazars, etc. – are powered by a common engine, accretion at a rate of a few solar masses per year into a supermassive black hole of several billion $M_\odot$ (Blandford & Rees 1974; Antonucci 1993). The differences relate to the mass and rotation rate of the hole, the environment in which it accretes, and the angle at which one observes. We suggest here that a similarly large variety of energetic phenomena can also be powered by accretion at a much higher rate into a small, stellar mass black hole. It could be that GRBs are but the "tip of the iceberg" and that many other interesting kinds of events await discovery.

In this paper, we have drawn attention to the possibility of two kinds of hyper-accreting black hole scenarios for making supernovae and high energy transients. Type I collapsars, as explored previously by MW99, have black holes that form promptly. The black holes in Type II collapsars, on the other hand, form after some delay owing to the fall back from a supernova lacking adequate energy to eject all of its helium core and heavy elements. Table 3 outlines the diverse phenomena resulting from the two collapsar types occurring in stars with varying radii.

We have shown (Fig. 11) that explosions of nearly constant total energy can have highly variable "equivalent isotropic energy" dependent not only upon the angle at which they are viewed, but also upon how passage through the star acts to collimate (or de-collimate) the jet. This should be true of both Type I and Type II collapsars. For the roughly 10 GRBs for which redshifts and GRB energies had been determined as of July, 1999, the inferred energy has an enormous range - from about 8×10^{47} erg for GRB 980425 (Galama et al.

1998) to several times 10^{54} erg for GRB 990123 (Kulkarni et al. 1999). Yet, as MW99 pointed out, the total explosion energy for both these events may have been $\sim 10^{52}$ erg with the energy collimated into a tight jet for GRB 990123 (see also Fig. 11 and Table 2) and dissipated in producing a powerful supernova for GRB 980425 (Iwamoto et al. 1998; Woosley, Eastman, & Schmidt 1999). The collimation properties of the jet may be more important than its total energy in determining the observed properties of a GRB.

We continue to support the view of MW99 that common, long hard GRBs (mean duration 20 s) seen by BATSE are produced in Type I collapsars. The GRB commences only after the jet has drilled a hole through the star (5 - 10 s) so that it can expand freely. The jet may be energized either by neutrino energy transport from the disk or by MHD processes. However, we also see the possibility of a number of other phenomena in Type II collapsars depending upon the collimation of the jet, the duration and mass of the accretion, and the nature of the presupernova star (see also Table 3).

"Smothered" and broadly beamed gamma-ray bursts; GRB 980425 - These occur in helium stars in which the jet either fails to maintain sufficient collimation (e.g., is too "hot" compared to the star through which it propagates), or loses its energy input before breaking out of the star ($\lesssim$10 s; MW99, MacFadyen & Woosley 1998). An energetic supernova still occurs (SN 1998bw, in this case) and a weak GRB is produced, not by the jet itself, but by a strong, mildly relativistic shock from break out ($\Gamma \sim 5$)interacting with the stellar wind (Woosley, Eastman, & Schmidt 1999). Kulkarni et al. (1998) and Wieringa, Kulkarni, & Frail (1999) have also argued that the radio emission from GRB 980425 was not strongly beamed and had a total energy not too much greater than the GRB ($\lesssim 10^{49}$ erg) suggesting that GRB 980425 was *not* a much more powerful GRB observed from the side (as in e.g., Nakamura 1999). Because these events are so low in gamma-ray energy, many could go undetected by BATSE and these could be the most common form of GRB in the universe. Because the initial jet may be less effectively collimated in GRBs made by supernova fallback, it is tempting to associate these phenomena with delayed black hole formation and the stronger GRBs with prompt black hole formation. More study is needed, but we tentatively offer Model J22 in Fig. 11 as a possible prototype for SN 1998bw. This model at 500 s post-bounce would appear essentially as a $\sim 10^{52}$ erg He core explosion with a small (10°) hole along each axis. A "hotter" jet, lower disk mass, or larger efficiency factor, ϵ, might provide even better agreement.

Long gamma-ray bursts; $\tau_{\rm burst} \gtrsim 100\ s$ - Though typical "long, complex bursts" observed by BATSE last about 20 seconds, there are occasionally much longer bursts. For example, GRB950509, GRB960621, GRB961029, GRB971207, and GRB980703 all lasted over 300

s. These long durations may simply reflect the light crossing time of the region where the jet dissipates its energy (modulo Γ^{-2}), especially in the "exterior shock model" for GRBs. However, if the event is due to internal shocks, the duration depends on the time the engine operates. Such long bursts would imply enduring accretion on a much longer time scale than one expects in the Type I collapsar model where the black hole forms promptly. The fallback powered models discussed in this paper could maintain a GRB for these long time scales (Fig. 6). Indeed considerable power may still be developed by the GRB days after the initial event with a luminosity declining roughly as $t^{-5/3}$ (Fig. 5).

Very energetic supernovae - SN 1997cy - Germany et al. (1999) have called attention to this extremely bright supernova with an unusual spectrum. The supernova was Type IIn and its late-time light curve, which approximately followed the decay rate of ^{56}Co, would require $\gtrsim$2 $M_\odot$ of ^{56}Ni to explain its brightness. Perhaps this was a pair-instability supernova (Woosley & Weaver 1982; Heger & Woosley 2000). On the other hand, circumstellar interaction could be the source of the energy and the agreement with $\tau_{1/2}(^{56}\mathrm{Co})$ merely fortuitous. This would require both a very high explosion energy and a lot of mass loss just prior to the supernova. The sort of model, described in Section 4.2, especially Model J22, could provide the large energy in a massive star that would be naturally losing mass at a high rate when it died. Large quantities of ^{56}Ni might also be made by the wind from the accretion disk (see below). But the presupernova radius of this event was too large and the jet would have shared its energy with too great a mass to make a common GRB. In Section 5, we placed a limit of $\Gamma \lesssim 2.5$ on any relativistic ejecta in such events. We thus regard the detection of a short, hard GRB from the location of SN 1997cy as spurious.

Nucleosynthesis - ^{56}Ni and the r-process - An explosion of 10^{52} erg focused into 1% of the star (or 10^{53} erg into 10%) will have approximately the same shock temperature as a function of radius as an isotropic explosion of 10^{54} erg. From the simple expression $\frac{4}{3}\pi r^3 a T^4 \sim 10^{54}$ erg (Woosley & Weaver 1995), we estimate that a shock temperature in excess of 5 billion K will be reached for radii inside 4×10^9 cm. The mass inside that radius external to the black hole (assumed mass initially 2 $M_\odot$) depends on how much expansion (or collapse) the star has already experienced when the jet arrives. Provided the star has not expanded much before the jet arrives, an approximate number comes from the presupernova model, 3 $M_\odot$ times the solid angle of the explosion divided by 4π, or $\sim$0.1 $M_\odot$. Additional ^{56}Ni will be synthesized by the wind blowing off the accretion disk (MW99; Stone, Pringle, & Begelman 1999) and this may be the dominant source in supernovae like SN 1998bw. Even for the relatively low accretion rates in Type II collapsars, the temperature in the accretion disk is hot enough to photodisintegrate the accreting matter

to nucleons (Popham et al. 1999). As this material expands and cools, it will reassemble mostly to ^{56}Ni. Stone et al. estimate that an appreciable fraction of the accreted matter will be ejected in such a wind.

The composition of the jet itself depends upon details of its acceleration that are hard to calculate. However it should originate from a region of high density and temperature (Popham et al. 1999). The high density will promote electron capture and lower $Y_{\rm e}$. The high entropy, low Y_e, and rapid expansion rate are what is needed for the r-process (Hoffman, Woosley, & Qian 1997). The mass of the jet, $\sim 10^{-4}$ M$_\odot$ (corrected for relativity) is enough to contribute significantly to the r-process in the Galaxy even if the event rate was $\lesssim$1% that of supernovae and the jet carried only a fraction of its mass as r-process.

Soft and hard x-ray transients from shock breakout - Focusing a jet of order 10^{52} ergs into 1 - 10% of the solid angle of a supernova results in a shock wave of extraordinary energy (Fig. 11). As it nears the surface of the star, this shock is further accelerated by the declining density gradient. We have estimated (Section 5, Fig. 13) that as the shock erupts from the surface of the star one may have soft x-ray transients of luminosity up to $\sim 10^{49}$ erg s^{-1} times the fraction of the sky to which high energy material is ejected (typically 0.01). The color temperature at peak would be approximately 2×10^6 K (see also Matzner & McKee 1999). A 10^{53} erg shock gave a transient about half as hot and ten times longer and fainter. The impact of the mildly relativistic matter could give an enduring x-ray transient like the afterglows associated with some GRBs, even though the time scale is too long for the x-ray burst to be a common GRB itself.

Supernova remnants with unusual symmetry - The expanding remnant of a supernova exploded by a jet should lack spherical symmetry. Along the rotational axis of the presupernova star matter expands with much greater velocity than along the equator. Dependent upon details of the circumstellar shock interaction, this could either lead to an elongated nebula characteristic of bipolar outflow or a torus of slower moving, denser debris in the equator. The massive stars that produce collapsars have a very high abundance of oxygen, so one might seek either toroidal or bipolar SNRs that are oxygen-rich. Lasker (1980) pointed out that N132D in the LMC might be such a remnant. More recent analysis (Sutherland & Dopita 1995; Morse, Winkler, & Kirshner 1995) suggests that the remnant may have elliptical structure. Another SNR with toroidal structure is E0102-72 in the SMC recently studied by the Chandra X-Ray Astronomy Facility.

Mixing in supernovae - SN 1987A - It is generally agreed (Arnett et al. 1989) that the

explosion that gave rise to SN 1987A initially produced a neutron star of approximately 1.4 $M_\odot$. There may have been $\sim$0.1 $M_\odot$ of fallback onto that neutron star (Woosley 1988) and a black hole may or may not have formed. Again invoking our *ansatz* that $L_{jet} = \epsilon \dot{M} c^2$, even for $\epsilon \sim 0.003$, we have a total jet energy of 6×10^{50} erg. This is about half of the total kinetic energy inferred for SN 1987A. Thus very appreciable mixing and asymmetry would be introduced by such a jet - *provided the material that fell back had sufficient angular momentum to accumulate in a disk outside the compact object.* However this would not be enough energy to make a powerful gamma-ray burst as proposed by Cen (1999). The radio and x-ray afterglow that one might expect from the impact of such a jet on the circumstellar medium was also not observed.

Still to be discovered - It may be that, especially with common GRBs, we have just seen the "tip of the iceberg" of a large range of high energy phenomena powered by hyper-accreting, stellar mass black holes. We already mentioned the possibility of a large population of faint, soft bursts like GRB 980425. Other possibilities include very long GRBs below the threshold of BATSE, "orphan" x-ray afterglows from jet powered Type II supernovae, GRBs from the first explosions of massive stars after recombination, and more. It is an exciting time.

The authors gratefully acknowledge helpful conversations on the subjects of gamma-ray bursts with Chris Fryer, David Meier, Ewald Müller, and Martin Rees. We also thank the anonymous referee for useful comments. This work has been supported by NASA (NAG5-8128 and MIT SC A292701), the NSF (AST 97-31569 and INT-97-31569), and the Department of Energy ASCI Program (W-7405-ENG-48), and by the Alexander von Humboldt-Stiftung (1065004). We are also grateful to the Max Planck Institut für Astrophysik for its hospitality while the final draft of this paper was prepared.

REFERENCES

Aloy, M. A., Ibanez, J. M., Marti, J. M., & Müller, E. 1999, ApJS, 122, 151

Aloy, M. A., Ibanez, J. M., Marti, J. M., Müller, E. & MacFadyen, A. I. 2000, ApJL, 531, 119

Antonucci, R. A. 1993, ARAA, 31, 473

Arnett, W. D., Bahcall, J. N., Kirshner, R. P., & Woosley, S. E. 1989, ARAA, 27, 629

Bethe, H. A. 1990, Rev. Mod. Phys., 62, 801

Blandford, R. A., & Rees, M. J. 1974, MNRAS, 169, 395

Blandford, R. D., & Znajek, R. L. 1977, MNRAS, 179, 433

Blandford, R. D., & Payne, D. G. 1982, MNRAS, 199, 833

Blinnikov, S. 1999, private communication

Cen, R. 1999, ApJL, 524, 51

Chevalier, R. A. 1982, ApJ, 259, 302

Chevalier, R. A. 1989, ApJ, 346, 847

Colgate, S. A. 1969, CanJPhys, 46, s476

Colgate, S. A. 1971, ApJ, 163, 221

Colgate, S. A. 1974, ApJ, 187, 333

Ensman, L. M., & Burrows, A. S. 1992, ApJ, 393, 742

Fransson, C. 1984, A&A, 133, 264

Fryer, C. L. 1999, ApJ, in press, astro-ph/9902315 astro-ph/9904122

Fryer, C. L., Benz, W., & Herant, M. 1996, ApJ, 460, 801

Fryer, C. L., Woosley, S. E., & Hartmann, D. H. 1999, ApJ, 526, 152

Fryxell, B. A., Müller, E., & Arnett, W. D. 1989, MPA Report 449, Garching, Germany

Fryxell, B. A., Müller, E., & Arnett, W. D. 1991, ApJ, 367, 619

Galama, T., et al. 1998, Nature, 395, 670

Germany, L., Reiss, D. J., Sadler, E. M., Schmidt, B., & Stubbs, C. W. 1999, ApJ, 533, 320

Gnatyk, B. L. 1985, Soviet Astronomy Letters, 11, 331

Heger, A. & Woosley, S. E. 2000 ApJ, in preparation

Heger, A., Woosley, S. E., & Langer, N. 2000, ApJ, in preparation

Hoffman, R. D., Woosley, S. E., & Qian, Y. 1997, ApJ, 482, 951

Imshennik, V. S., & Nadyozhin, D. K. 1989, in *Supernova 1987A*, Ap and Spac Sci Rev, 8, Part 1, p. 49ff

Iwamoto, K., et al. 1998, Nature, 395, 672

Janka, H. -Th., Ruffert, M.m & Eberl, T. 1999a, in *Nuclei in the Cosmos, V*, eds. N. Prantzos and S. Harissopulos, (Editions Frontieres: Paris), p. 325, astro-ph/9810057

Janka, H. -Th., Eberl, T., Ruffert, Mm., & Fryer, C. 1999b, ApJL, 527, 39

Katz, J. 1997, ApJ, 490, 633

Khokhlov, A. M., Höflich, P. A., Oran, E. S., Wheeler, J. C., Wang, L., & Chtchelkanova, A. Yu., 1999, ApJL, 524, 107

Koide, S., Shibata, K., & Kudoh, T. 1998, ApJL, 495, L63

Koide, S., Meier, D. L., Shibata, K., & Takahiro K. 1999, ApJ, 536, 668

Krasnopolsky, R., Li, Z-Y., Blandford, R., 1999, ApJ, 526, 631

Kulkarni, S. R., Frail, D. A., Wieringa, M. H., Ekers, R. D., Sadler, E. M., Wark, R. M., Higdon, J. L., Phinney, E. S., & Bloom, J. S. 1998, Nature, 395, 663

Kulkarni, S. R., Djorgovski, S. G., Odewahn, S. C., Bloom, J. S., et al. 1999, Nature, 398, 389

Lasker, B. M. 1980, ApJ, 237, 765

Lee, H. K., Wijers, R.A.M.J., & Brown, G. E. 1999, Physics Reports, 325, 83

Leising, M. D., et al. 1994, ApJL, 432, L95

Livio, M. 1999, Phys Rept, 311, 225

Livio, M., Ogilvie, G. I., & Pringle, J. E. 1999, ApJ, 512, 100

MacDonald, D. A., Thorne, K. S., Price, R. H., & Zhang, X.-H. 1986, in *Black Holes: The Membrane Paradigm*, ed. K. Thorne, R. Price, and D. MacDonald, (Yale University Press, New Haven), p. 121

MacFadyen, A., & Woosley, S. E. 1998, BAAS, 30, No. 4, 1311, see also http://www.itp.ucsb.edu/online/gamma_c99/woosley/

MacFadyen, A., & Woosley, S. E. 1999, ApJ, 524, 262 (MW99)

Matzner, C. D., & McKee, C. F. 1999, ApJ, 510, 379

McKee, C. R. & Colgate, S. A 1973, ApJ, 181, 903

Meier, D. L., Edgington, P., Godon, P., Payne, D. G., & Lind, K. R. 1997, Nature, 388, 350

Meier, D. L. 1999, ApJ, 522, 753

Mészáros, P. 1999, Proc. 19th Texas Symposium, Nuc. Phys. B, in press, astro-ph/9904038

Mészáros, P., & Rees, M.J., 1997, ApJL, 482, L29

Morse, J. A., Winkler, P. F., & Kirshner, R. P. 1995, AJ, 109, 2104

Müller, E. & Steinmetz, M. 1995, Computer Physics Communications, 89, 45

Müller, E., Aloy, M. A., Ibanez, J. M., Marti, J. M., & MacFadyen, A. 2000, Gamma-Ray Bursts: 5th Huntsville Symposium, eds. Kippen, R.M. et al. , p.565 (AIP)

Nakamura, T. 1999, ApJL, 522, L101

Piran, T. 1999, Physics Reports, 314, 575.

Popham, R., Woosley, S. E., & Fryer, C. 1999, ApJ, 518, 356

Pringle, J. E. 1993, in *Astrophysical Jets*, eds. D. Burgarella, M. Livio, and C. P. O'Dea, Cambridge Univ Press, p. 1

Stone, J. M., Pringle, J. E., Begelman, M. C. 1999, MNRAS, 310, 1002

Sutherland, R. S., & Dopita, M. A. 1995, ApJ, 439, 365

Thompson, C. 1994, MNRAS, 270, 480

Usov, V. 1994, MNRAS, 267, 1035

Weaver, T. A., Zimmerman, G. B., & Woosley, S. E. 1978, ApJ, 225, 1021

Wheeler, J. C., Yi, I., Höflich, P., & Wang, L. 1999, ApJ, in press, astro-ph/9909293

Wieringa, M. H., Kulkarni, S. R., & Frail, D. A. 1999, Astron & Ap Supp, 138, 467

Woosley, S. E. 1988, ApJ, 330,218

Woosley, S. E. 1993, ApJ, 405, 273

Woosley, S. E., & Weaver, T. A. 1982, in *Supernovae: A Survey of Current Research*, eds. M.J. Rees and R.J. Stoneham, Dordrecht: Reidel, p.. 79

Woosley, S. E., & Weaver, T. A. 1995, ApJS, 101, 181

Woosley, S. E., Eastman, R. G., Schmidt, B. P. 1999, ApJ, 516, 788

Woosley, S. E., MacFadyen, A. I., & Heger, A. 1999, to be published in: Supernovae and Gamma-Ray Bursts, eds. M. Livio, K. Sahu, & N. Panagia (Cambridge: Cambridge University Press), astro-ph/9909034

Zampieri, L., Colpi, M., Shapiro, S. L., Wasserman, I. 1998, ApJ, 505, 876

Table 1. Explosion energy and fallback.

run	$\alpha_{\rm pist}$	explosion energy[a] (10^{51} erg)	KEP fallback ($M_\odot$)	PPM fallback ($M_\odot$)	$t_{1/2}$[b] (s)
A01	0.025	0.255	3.71	3.63	100
A02	0.05	0.341	3.41	3.35	145
A03	0.10	0.479	3.03	3.00	265
A04	0.15	0.595	2.85	2.64	450
A05	0.20	0.702	2.52	2.23	730
A06	0.25	0.805	1.96	1.73	1060
A07	0.30	0.906	1.39	1.22	1140
A08	0.35	1.007	0.91	0.83	890
A09	0.40	1.105	0.60	0.60	940
A10	0.42	1.152	0.53	0.53	1000
A11	0.44	1.207	0.48	0.47	1060
A12	0.50	1.326	0.24	0.33	1240
A13	0.60	1.507	0	0.18	1310
A14	0.70	1.682	0	9.8(-2)	970
A15	0.80	1.850	0	6.2(-2)	610
A16	0.95	2.092	0	3.7(-2)	440
A17[c]	0.025	0.316	3.37	-	-
B01	0.20	0.314	5.2	-	-
B02	0.30	0.415	4.9	-	-
B03	0.40	0.513	4.6	-	-
B04	0.60	0.726	3.1	-	-
B05	0.70	0.835	2.1	-	-
B06	0.75	0.913	1	-	-
B07	0.80	0.960	0.06	-	-
B09	0.95	1.143	0.05	-	-
B10	1.00	1.200	0	-	-

[a]Final kinetic energy of the ejecta at infinity.

[b]Time scale to accrete half of total accreted mass.

[c]Final piston radius of 10^{10} cm.

Table 2. Explosion Characteristics at t = 400 s After Jet Initiation

Name	ϵ	f_P	Δ M ($M_\odot$)	E_{tot} (10^{51} ergs)	R($\theta > 10°$)	R($\theta > 20°$)
J33	0.001	0.001	2.76	3.38	0.075	0.037
J32	0.001	0.01	2.69	3.23	0.102	0.047
J31	0.001	0.1	2.51	3.00	0.425	0.256
J22	0.01	0.01	1.72	19.91	0.429	0.230

Table 3. Observable phenomena resulting from collapsars.

	Type I	Type II
Black Hole formation	prompt ~ 1 s	delayed $30 - 3000$ s
$\dot{M}(\mathrm{M}_\odot\ \mathrm{s}^{-1})$	~ 0.1	$0.0001 - 0.01$
$\tau^*_{\rm accretion}$	~ 10 s	$30 - 3000$ s
No H envelope Wolf-Rayet star	$t_{\rm engine} > t_{\rm bo}$ GRB + Type Ib/c SN	$t_{\rm engine} > t_{\rm bo}$ long GRB + Type Ib/c SN
Small H envelope Blue supergiant	$t_{\rm engine} < t_{\rm bo}$ Type II SN; XRT	$t_{\rm engine} \gtrsim t_{\rm bo}$ long GRB? + Type II SN
Large H envelope Red supergiant	$t_{\rm engine} \ll t_{\rm bo}$ Type II SN XRT	$t_{\rm engine} \lesssim t_{\rm bo}$ Type II SN XRT

SN=supernova, collapsar supernovae are jet-driven and asymmetric; XRT=x-ray transient; $t_{\rm bo}$=time for jet to break out of stellar surface; $t_{\rm engine}(\approx \tau_{\rm accretion})$=time jet is powered.

* A small amount of accretion can continue for a long period after the explosion (see Fig. 5).

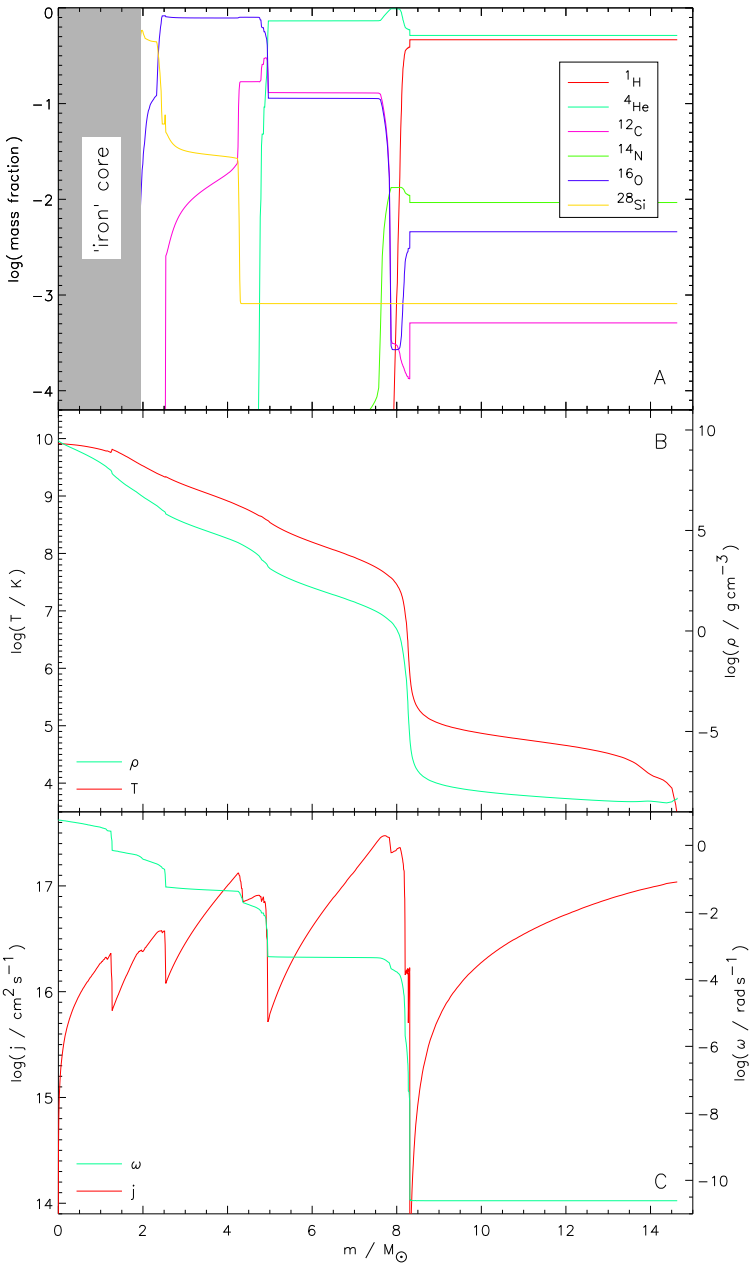

Fig. 1.— The presupernova model used for these studies, Model A, is derived from calculations of Heger, Woosley, & Langer (2000). This model was evolved with "restricted semiconvection", including the effects of rotation and an equatorial rotational velocity on the main sequence of 200 km s^{-1}. Panel A shows the composition of this initially 25 M$_{\odot}$ star, now reduced to 14.63 M$_{\odot}$ by mass loss. The iron core was removed for this study and replaced by a piston (Fig. 3). Panel B shows the characteristic red supergiant density and temperature structures of the presupernova star, especially the cool low density hydrogen envelope outside 8.4 M$_{\odot}$. The bottom panel shows the distribution of specific angular momentum and angular velocity in the presupernova star. The angular momentum in the equatorial plane is actually 50% higher than this angle-averaged value.

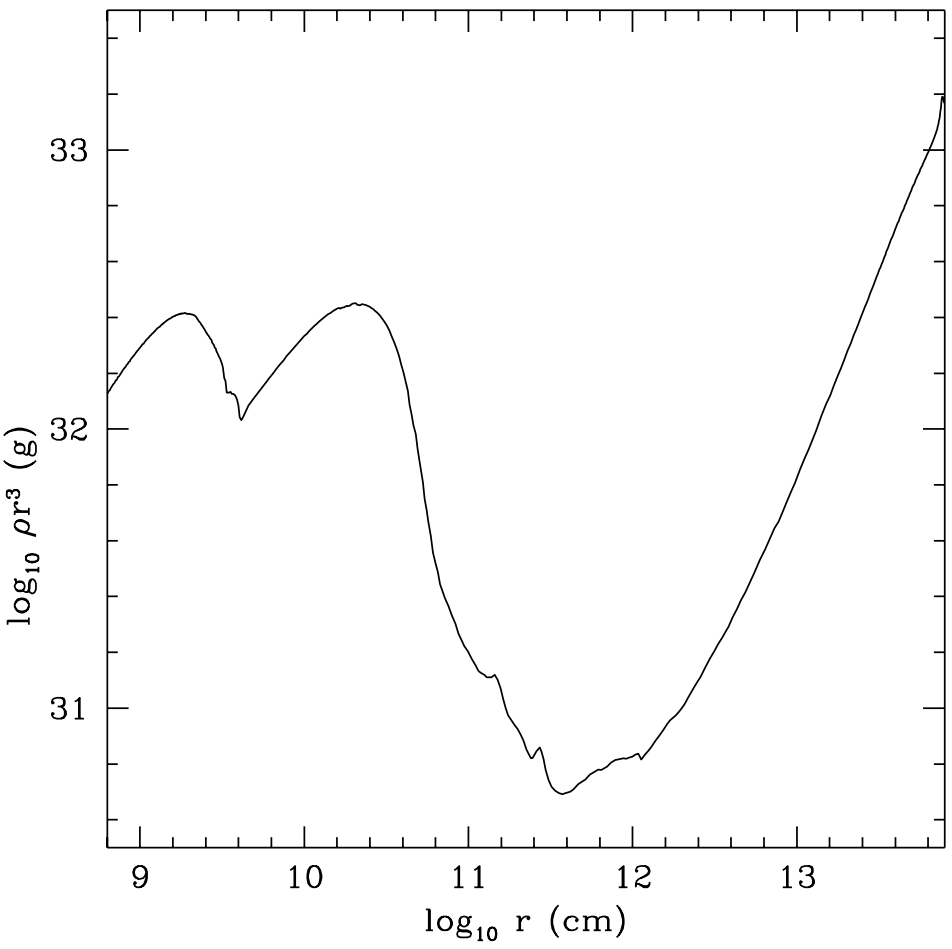

Fig. 2.— The distribution of the quantity ρr^3 in the presupernova model (Fig. 1). The supernova shock will speed up in regions of decreasing ρr^3 and slow in regions where ρr^3 increases. The large increase outside 10^{12} cm occurs in the hydrogen envelope. The dip at log r = 9.6 and 10.8 are the edges of the carbon-oxygen and helium cores.

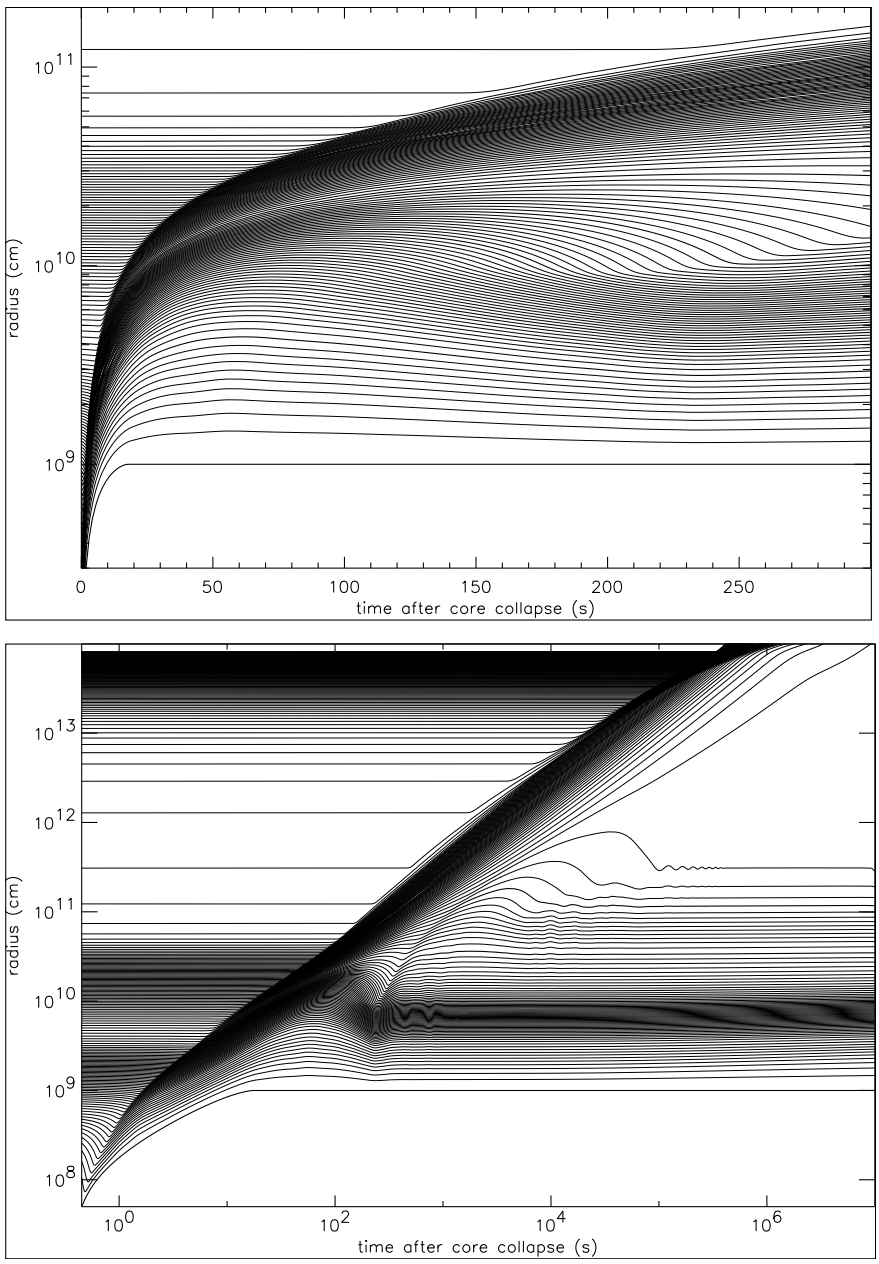

Fig. 3.— Radial history of Lagrangian mass shells in the KEPLER calculation of Model A01 (Table 1). Dark lines represent mass shells of 0.5 $M_\odot$, faint lines, 0.05 $M_\odot$. The piston (bottom-most dark line) moves out, launching the shock, and comes to rest, after 19.5 s, at 10^9 cm. The location of the supernova shock is visible as the outer boundary of the dark concentration of curved lines. All material on the grid moves outwards until 60 s after core bounce, when some begins to to fallback and come to rest on the piston. After about 150 s, an accretion shock has developed whose location is an artifact of the stationary piston. In the lower panel the supernova shock continues to the surface of the star, but a total of 3.71 $M_\odot$ eventually falls back to rest on the piston. The slope of the shock location gives its speed which decelerates in regions of increasing ρr^3. This model was linked to the PPM code 100 s after material had begun to fallback, but before any appreciable accumulation on the piston.

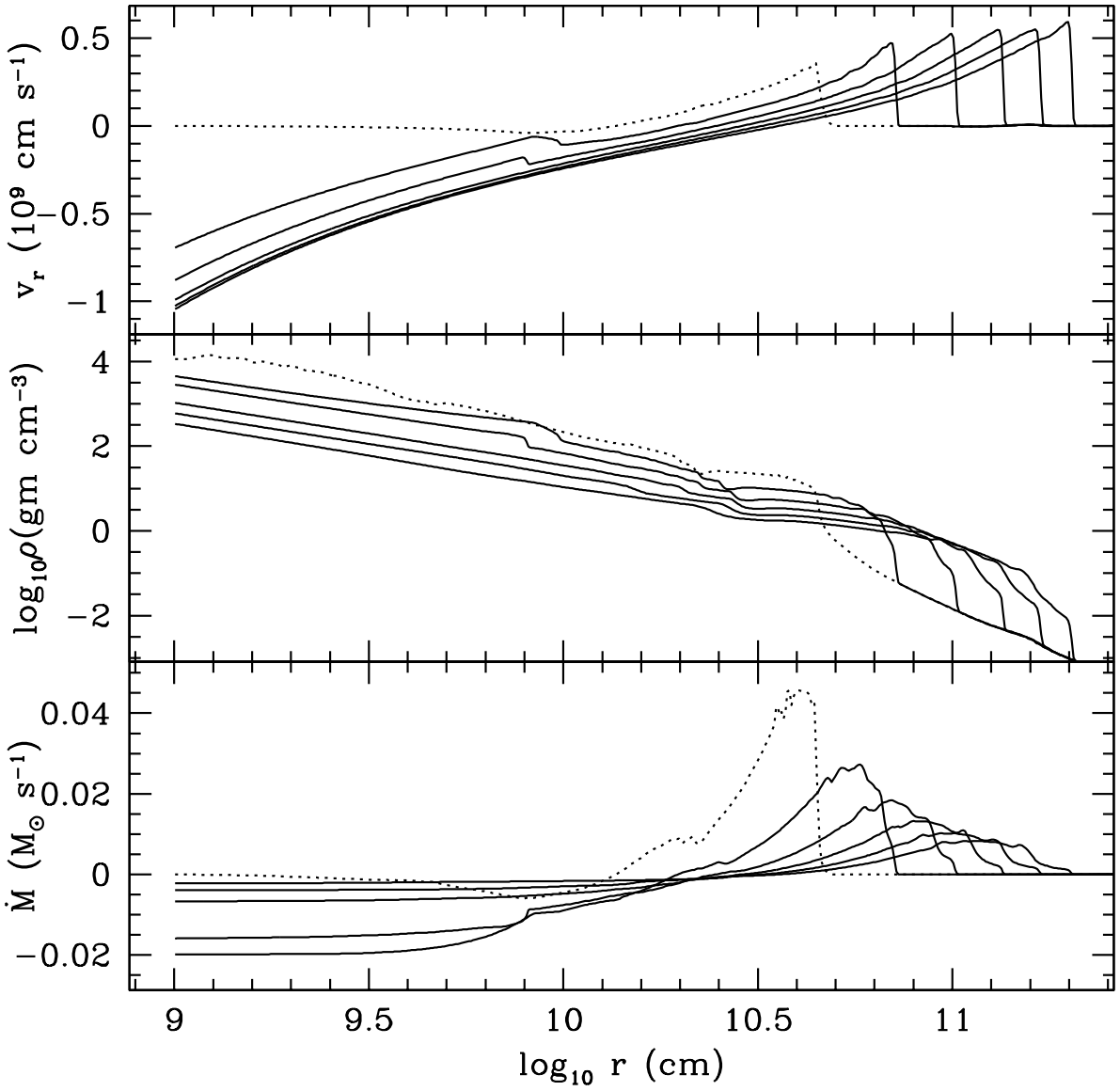

Fig. 4.— Propagation of the shock shown in Fig. 3 following the remapping of the problem into the one-dimensional PPM code at 100 s (dotted line). The solid lines show the velocity (10^9 cm s^{-1}), log density (g cm^{-3}), and accretion rate ($M_\odot$ s^{-1}) as a function of radius at intervals 50, 100, 150, 200, and 250 s after the remapping. During the first roughly 20 s the motion of matter is still influenced by memory of the KEPLER piston at 10^9 cm and is nearly stationary at small radii. Though the residual support of this material is artificial, only a small amount of mass accretes at this time, which may be thought of as the interval during which the loss of pressure at the origin due to black hole formation propagates to 10^9 cm. By 250 s after the remapping, (last solid line shown) the accretion rate has declined greatly (Fig. 5).

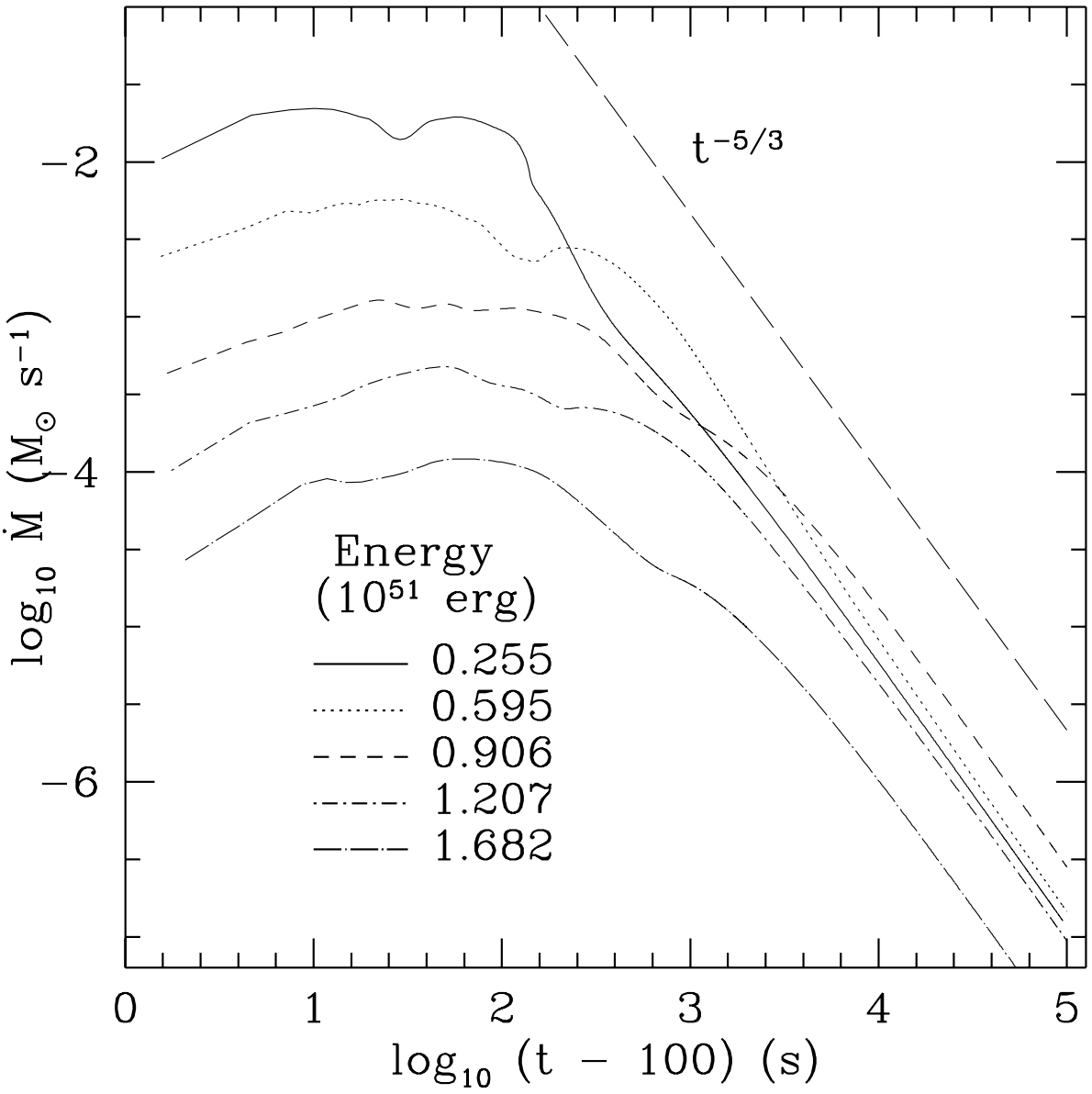

Fig. 5.— Accretion rates for fallback in five different explosions: A01 (solid), A04 (dotted), A07 (dashed), A11 (short dash-dot) A14 (long dash-dot) (Table 1). Calculations were carried out using a one-dimensional version of the PROMETHEUS PPM hydrodynamics code. Time is measured from the collapse of the iron core and accretion rate plotted as a function of the time since the calculation was linked to the PPM code at 100 s. At late times the accretion rate follows the $t^{-5/3}$ scaling suggested by Chevalier (1989).

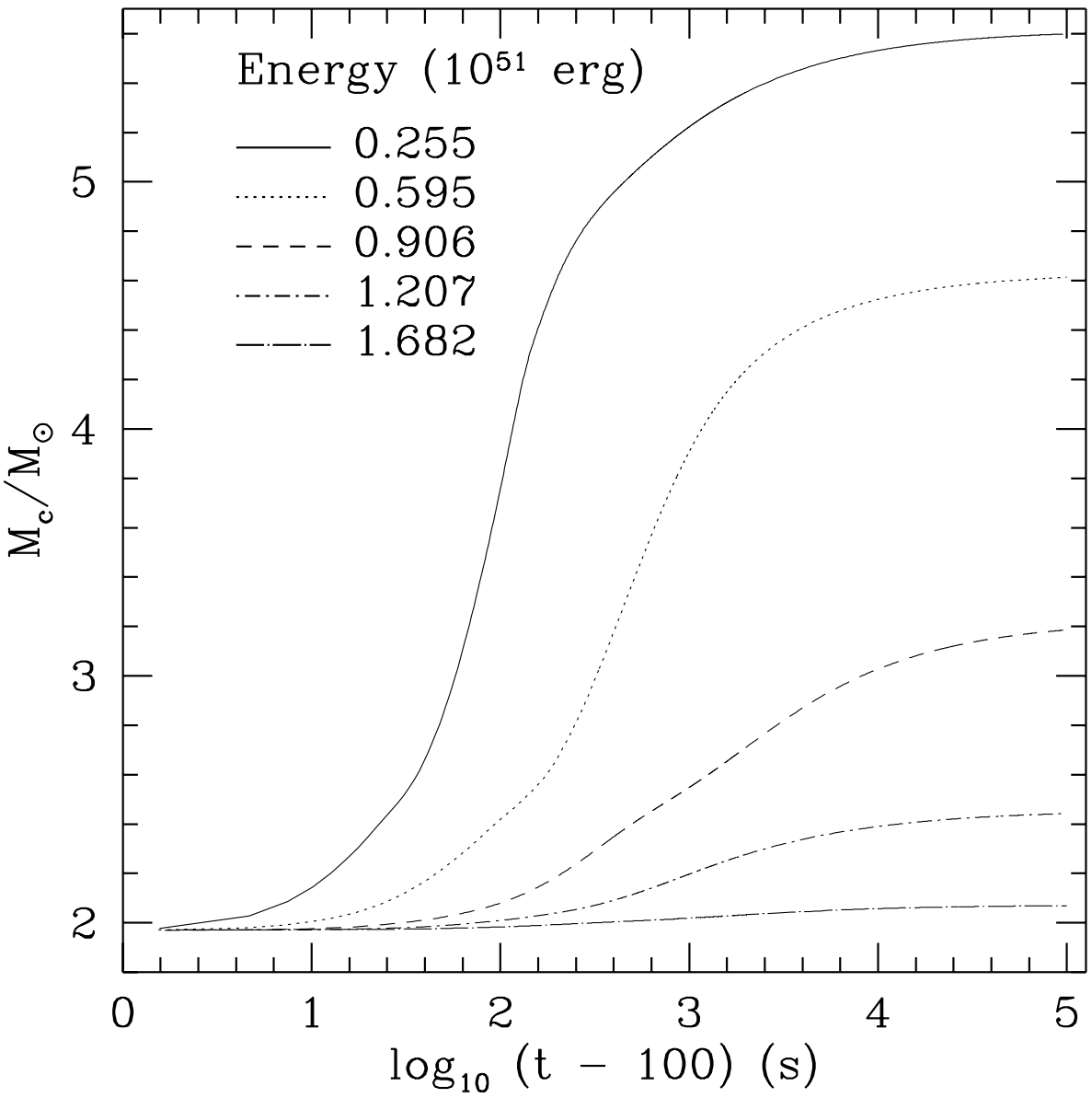

Fig. 6.— Accumulated mass as a function of time for the same calculations shown in Fig. 5.

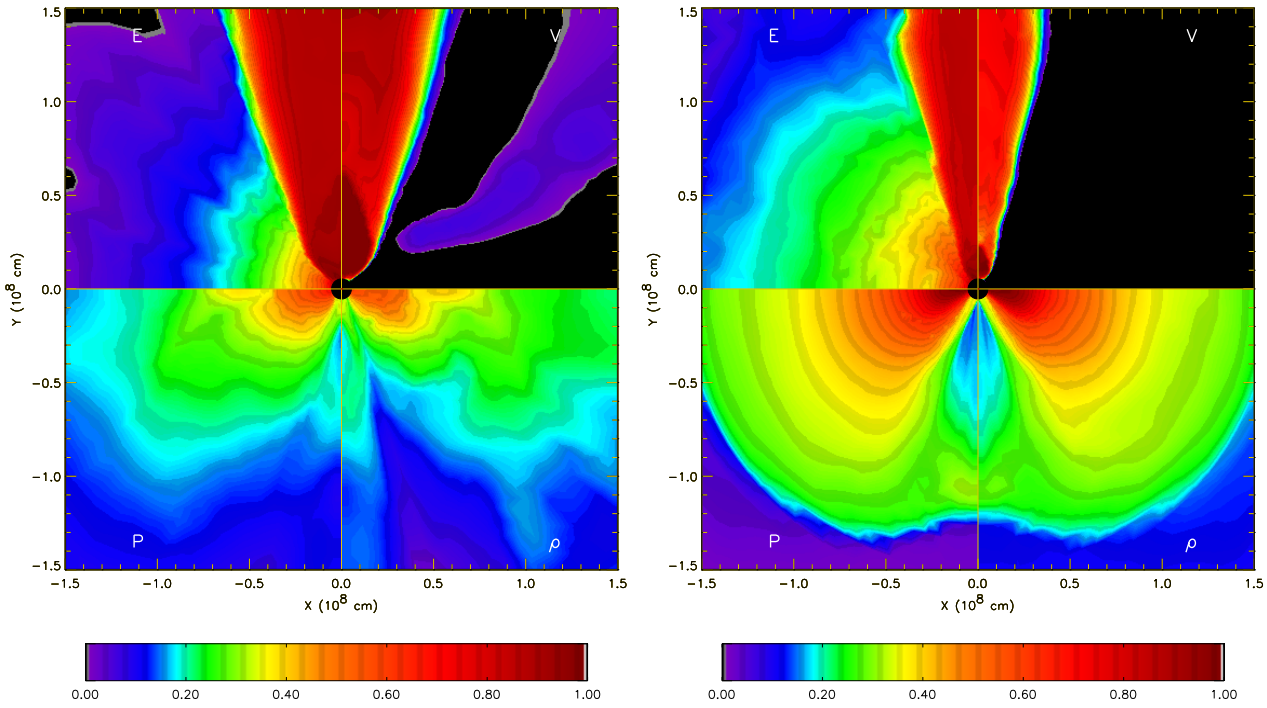

Fig. 7.— Hydrodynamical focusing of jets initiated in the collapsar disks of MW99 is shown here for two values of the disk viscosity parameter, $\alpha = 0.1$ (left) and 5×10^{-4} (right). Each jet was injected at 5×10^6 cm with an energy deposition rate of 1.8×10^{51} erg s^{-1}, roughly equally in internal and kinetic energy, and an opening half-angle of 10 degrees. The figures show the situation 0.6 s after the jets are turned on. The bottom two panels of each figure show the logarithms of the pressure (left) and density (right) for the disk before jet initiation. The mass of the disk is approximately two orders of magnitude smaller in the high viscosity case. The top two panels show the logarithm of total energy density (left) and the velocity (right) 0.6 s after the start of jet injection. The minimum and maximum values for internal energy are log E (erg g^{-1}) = 18.5 and 20.3, for velocity, v (cm s^{-1}) = 5.0×10^8 and 1.5×10^{10}, for density, log ρ (g cm^{-3})= 5 and 11.5, and for pressure, log P (dyne cm^{-2}) = 23 and 30.1. The color bar indicates the logarithmic interpolation between these two extrema. For example, the yellow-orange region of the density plot represents $\log \rho = 5 + 0.40(11.5 - 5) = 7.6$. The jet is clearly less well collimated in the high viscosity case, presumably because of the smaller mass of the disk and the weaker pressure gradients confining the flow to the polar region. Note also the presence of "plumes" of high outward velocity at about 45 degrees in the plot for the high viscosity case. See MW99 for discussion.

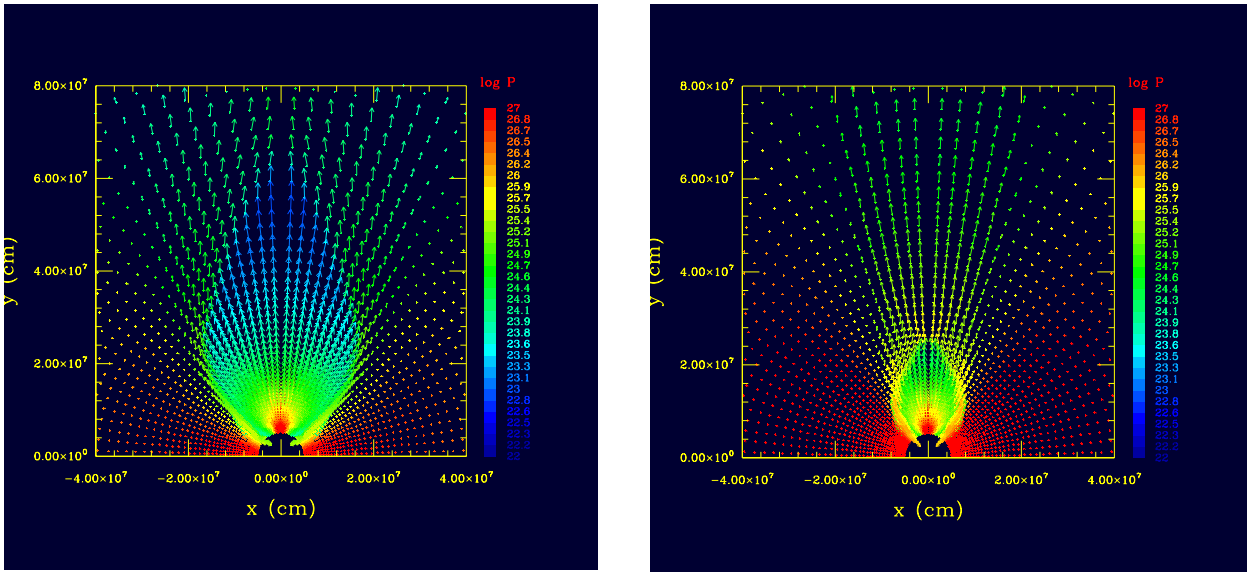

Fig. 8.— Further detail of the initial hydrodynamical focusing of the initial jets in the high (left) and low (right) disk viscosity cases (see Fig. 7). The pressure ranges from 10^{22} dyne cm^{-2} (dark blue) to 10^{27} dyne cm^{-2} (red) and the region plotted is the inner 400 km (x) by 800 km (y). The longest velocity vectors represent a speed of 1.5×10^{10} cm s^{-1}. Both plots are at a time 0.6 s after jet initiation. The lower density in the high viscosity case results in the jet being less well collimated. It expands laterally with approximately the sound speed, which for equal internal and kinetic energies is comparable to its radial speed. A jet with a higher fraction of internal energy would spread even more, especially if the disk mass were further reduced. The jet in the low viscosity calculation also propagates in a lower density medium and moves further before a shock develops.

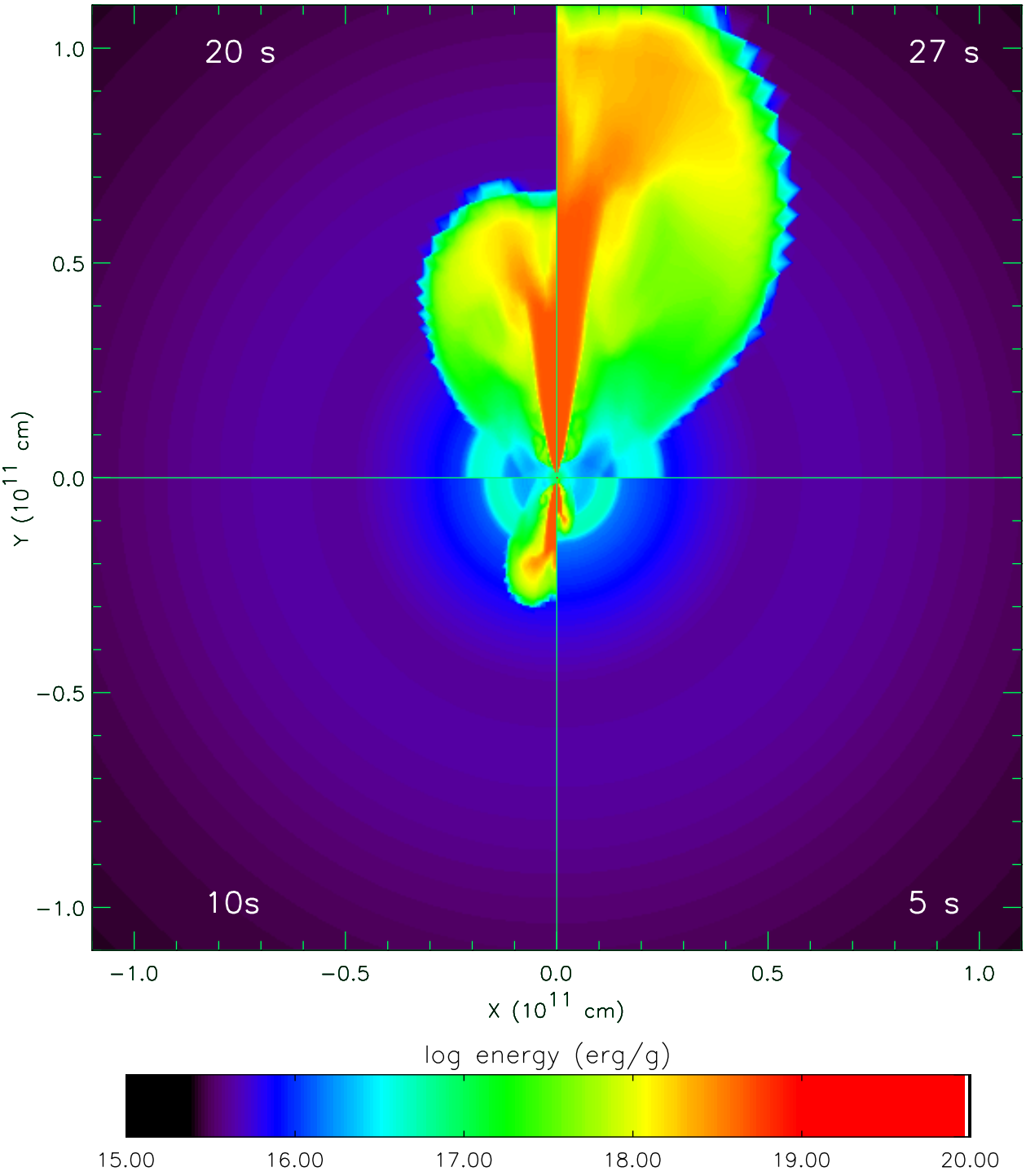

Fig. 9.— The specific energy density (internal plus kinetic) of the jet and explosion is shown at times of 5, 10, 20 and 27 s after initiation of the jet in Model J22 (Table 2). The passage of the jet initiates a shock that propagates to lower latitudes, eventually exploding the entire star. The original supernova shock can be seen as a pale blue circle at a radius of about 2×10^{10} cm.

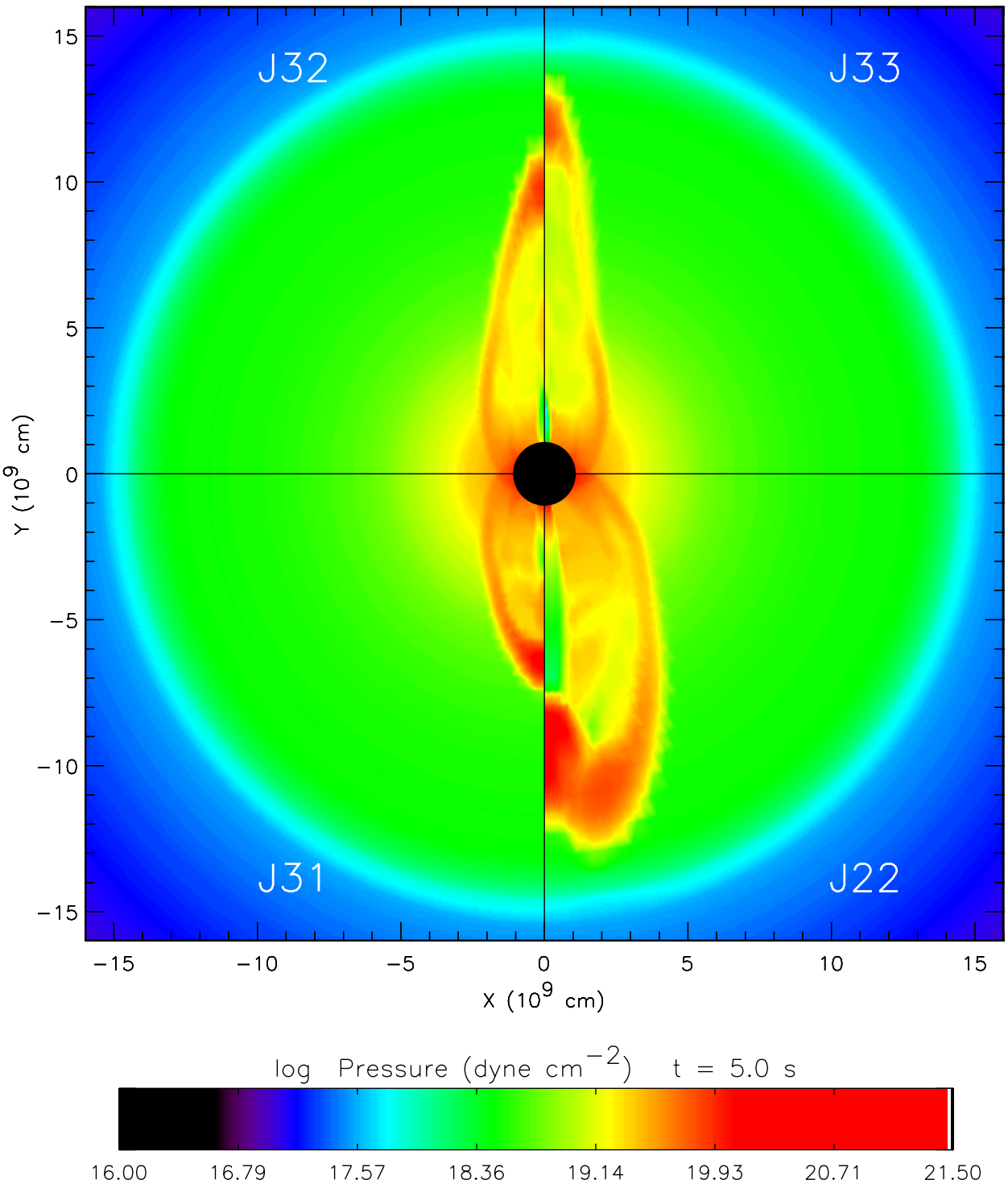

Fig. 10.— Pressure in the jet and surrounding star at 5.0 s after the initiation of the jet in four different models (Table 2). For the J3n series, higher pressure clearly leads to greater jet divergence, more mass swept up, and slower propagation. Model J22 had a higher jet energy than the other models. The edge of the helium core is at 5×10^{10} cm ($X_H = 0.01$; ρ = 0.6 g cm^{-3}), but the presupernova density begins to decrease rapidly below 100 g cm^{-3} outside of 1.4×10^{10} cm (the green disk in the figure).

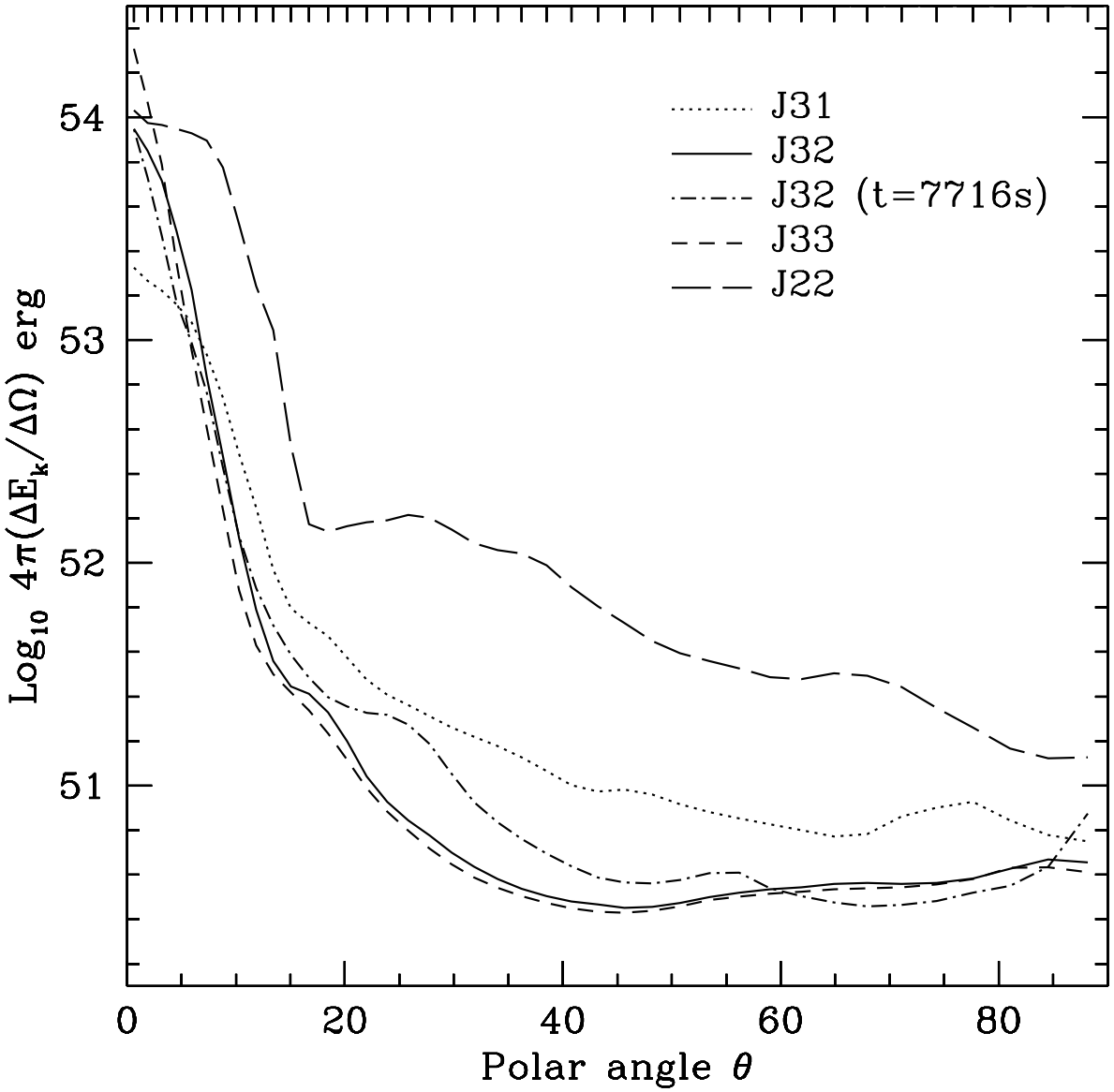

Fig. 11.— The "equivalent isotropic kinetic energy" as a function of polar angle for four models having variable energy efficiency factors and internal pressures (Table 2). Except for J32, the calculations are all sampled at 400 s after the initiation of the jet (500 s post-bounce). At this point the jets have exited the helium core and are moving through the hydrogen envelope. Model J32 is shown at two times, once at 400 s and later, at 7716 s, as the jet reaches the surface of the star at 8×10^{13}cm (dash-dot line). The collimation of Model J32 is further improved by its passage through the hydrogen envelope. Note that the degree of collimation is strongly dependent upon $f_{\rm P}$. Equivalent isotropic kinetic energy is defined as the integral from the center to surface of the star of its kinetic energy in the solid angle subtended by θ and $\theta + \Delta\theta$ divided by the solid angle, $2\pi(\cos\theta - \cos(\theta + \Delta\theta))$ and multiplied by 4π. The injected energy at the base of the jet would be a flat line out to ten degrees with a value equal to $66\,\epsilon\Delta{\rm M}c^2$ with ΔM in Table 1 and $66 = (1 - \cos(10^\circ))^{-1}$. Tick marks along the top axis give the angular zoning of the two dimensional code.

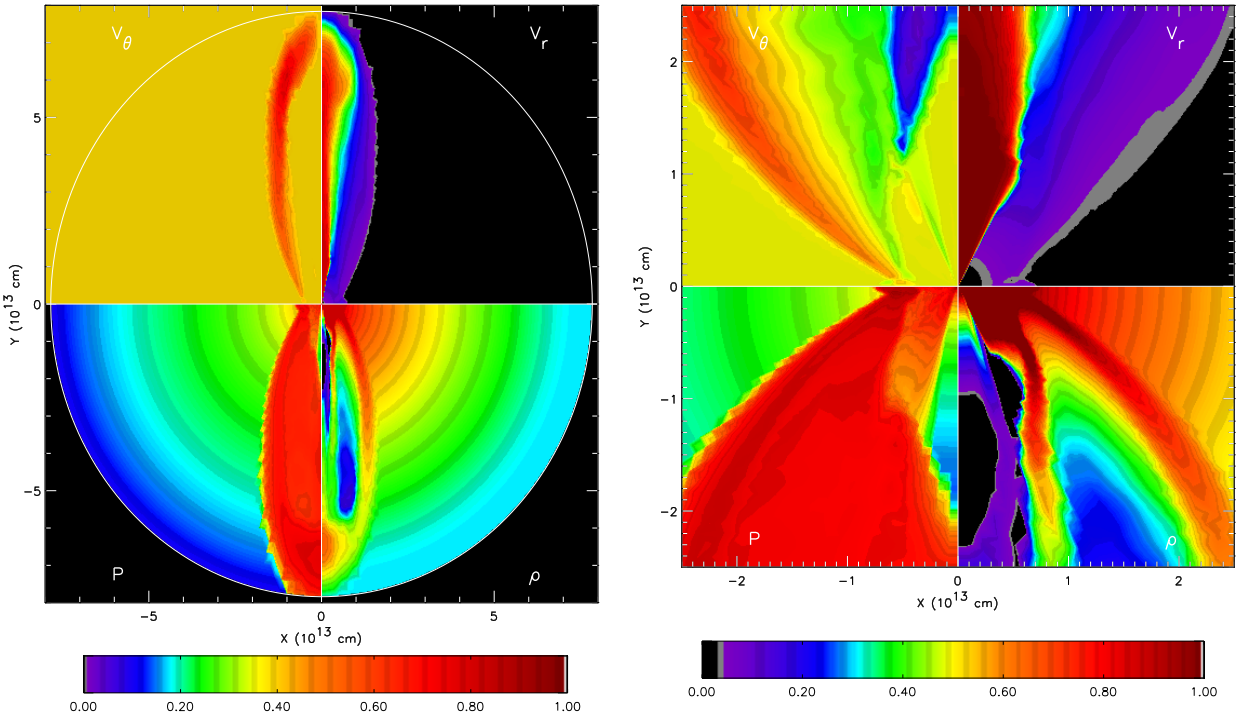

Fig. 12.— The structure of Model J32 as the jet nears the surface 7820 s after core collapse. The total explosion energy at this time is 4.1×10^{51} ergs at this time, probably a good approximation to the final value. The theta velocity, radial velocity and logarithms of density and pressure are given with the minimum and maximum values for v_θ are -1.5×10^9 and 1.5×10^9, for radial velocity, v_r, -6.7 $\times 10^7$ and 1.0 $\times 10^{10}$, for density, $\log_{10}\rho$, -9 and -6.8, and for pressure, $\log_{10}$ P, 2.5 and 10.9, all in cgs units. The colors indicate the interpolation scale between minimum and maximum (see Fig. 7). Positive v_θ is motion away from the polar axis ($\theta = 0$) along an arc of constant radius. The v_θ plot shows the expansion of the high pressure bubble blown by the jet sweeping around the star (red region) but also an inner region of collimation (blue, purple, and green). At $r = 7 \times 10^{13}$ cm the x-component of the velocity of the expansion shock is $v_x = 2.0 \times 10^9$ cm s^{-1} (compared to a sound speed of only 3×10^6 cm s^{-1}), while the y-component is $v_y = 9.6 \times 10^9$ cm s^{-1} resulting in an aspect ratio for the bubble between 0.2 and 0.3. The velocity and pressure plots show a collimation of the jet flow near 1×10^{13} cm, well into the hydrogen envelope of the star, and evacuation of a low density column by the jet. Not however, the plug of high density material being shoved along by the jet.

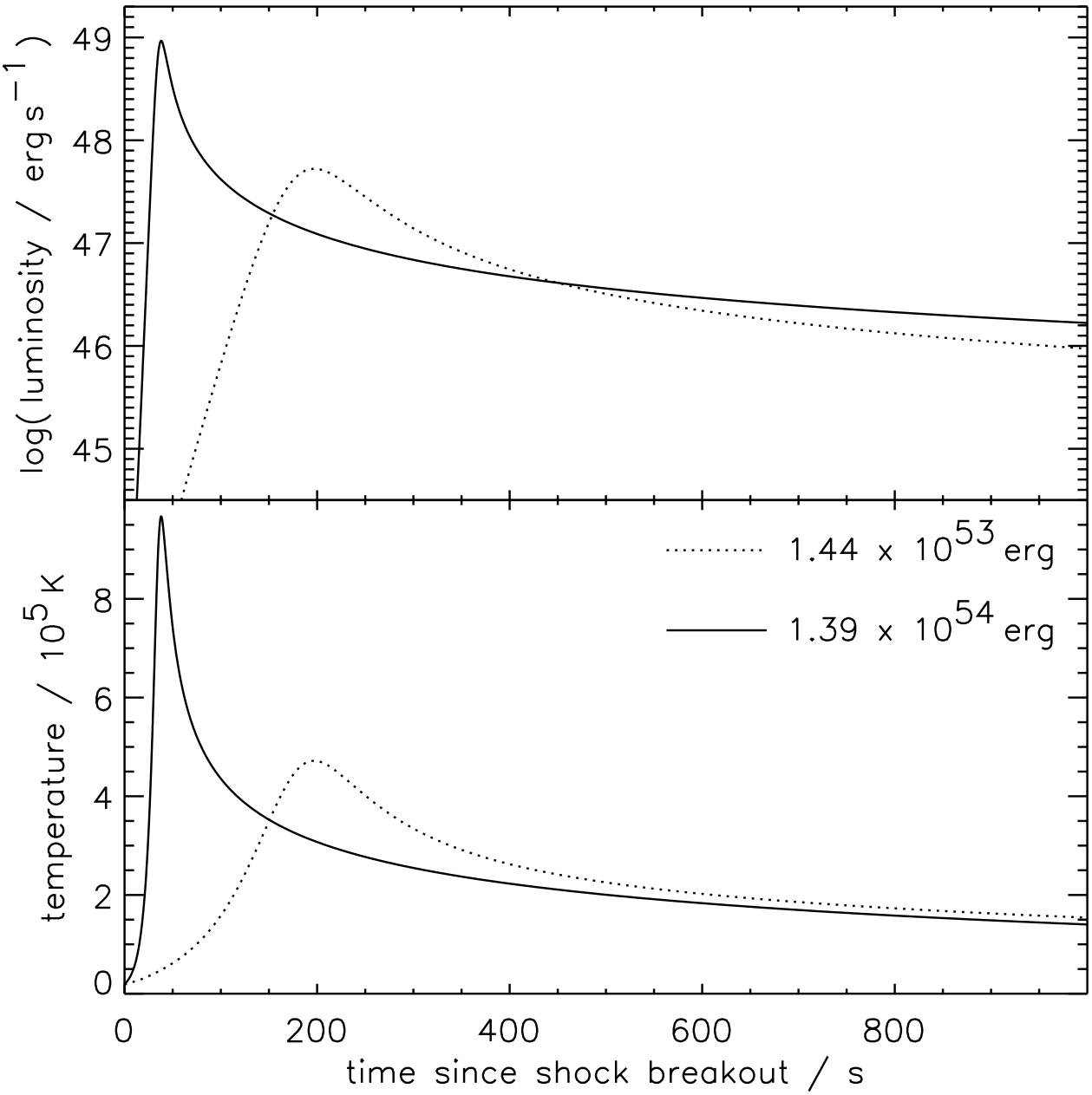

Fig. 13.— Shock breakout in spherically symmetric explosions for Model A for the KEPLER calculation of two cases of a 1.44×10^{53} erg explosion (dotted line) and a 1.39×10^{54}erg explosion (solid line) as a function of time since the onset of shock breakout. The upper panel gives the total luminosity and the lower panel the *effective* temperature, which probably underestimates the color temperature, T_c by about a factor of two to three. The FWHM of the luminosity curves are 12.5 and 94 s for low and high energy respectively. The widths of the temperature curves are 56 and 350 s.

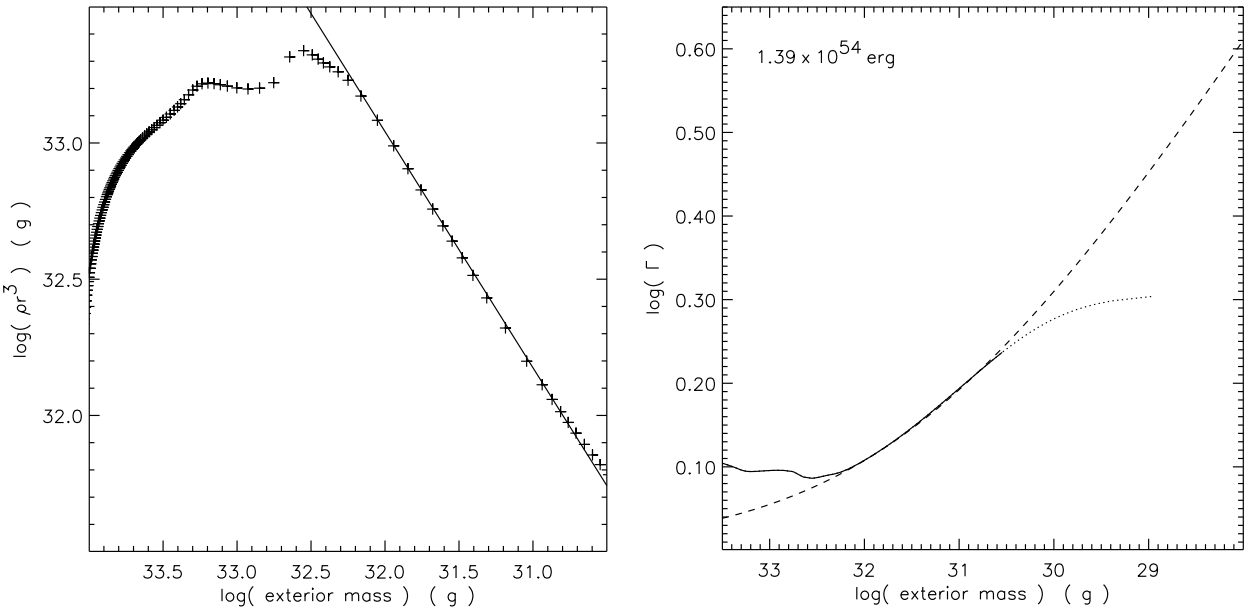

Fig. 14.— Density structure near the surface of the red supergiant (Model A) (left panel) and extrapolated Lorentz factor for the breakout of a shock of energy 1.39×10^{54} erg (right panel). Crosses show the product of density times r^3 for the hydrogen envelope and zones near the surface. A power law $\rho r^3 \propto (\Delta m)^{0.86}$ fits the surface of the Kepler model well. Using this density structure and the near constancy of $\Gamma\beta(\rho r^3)^{1/5} \approx 3.25 \times 10^6$ ($g^{1/5}$), one can extrapolate (dashed line) to obtain the relativistic Γ for mass zones outside of $10^{30.5}$ g. However the curve for Γ is not valid for external masses less than $10^{29.3}$ g (see text). The maximum Γ for this shock energy is thus $\Gamma \approx 2.5$. The curved dotted line at masses below $10^{30.7}$ shows the results one obtains using the actual density structure in KEPLER for optically thin zones rather than the extrapolation of ρr^3 in the left panel.